Unified theory of resistive and inertial ballooning modes in three-dimensional configurations

T. Rafiq*, C. C. Hegna, J. D. Callen, G. Bateman*, A. Y. Pankin* and A. H. Kritz*

Engineering Physics Department, University of Wisconsin, Madison, Wisconsin 53706-1609

June 16, 2008

Abstract

A linear stability theory of non-ideal MHD ballooning modes is investigated using a two fluid model for arbitrary three-dimensional electron-ion plasmas. Resistive-inertia ballooning mode (RIBM) eigenvalues and eigenfunctions are calculated for a variety of equilibria including axisymmetric shifted circular geometry ($\hat{s}-\alpha$ model) as well as for three dimensional configurations of interest relevant to the Helically Symmetric Stellarator (HSX). For typical HSX parameters, characteristic growth rates exceed the electron collision frequency. In this regime, electron inertia effects dominate plasma resistivity and produce an instability whose growth rate scales with the electromagnetic skin depth. However, the resistive and inertia effects become unimportant as the plasma β is increased close to the transition to an ideal mode. Analytic calculations of RIBM stability using a two scale analysis are presented. This work generalizes previous calculations used for axisymmetric $\hat{s}-\alpha$ geometry [R. H. Hastie, J. J. Ramos and F. Porcelli *Phys.Plasmas* **10,** 4405 (2003)] to general three-dimensional geometry. Both analytic and numerical results show that in the absence of drift effects RIBM modes are purely growing and persist in regimes where ideal MHD ballooning modes are stable. It is found that the magnitudes of the linear growth rates are not sensitive to the magnetic configuration that exists in HSX plasmas.

*Department of Physics, Lehigh University, 16 Memorial Drive East, Bethlehem Pennsylvania 18015

I. Introduction

Unstable resistive ballooning modes (RBMs) may play an important role in producing edge plasma fluctuations and anomalous transport in tokamaks and stellarators. RBMs have been extensively studied in axisymmetric tokamaks using linear ([1]-[6]) and nonlinear theories ([7]-[9]). However, only limited work on these instabilities in fully three-dimensional stellarator geometries has been published (for example, see Refs. [10]-[12]). Stellarator geometry is difficult because of its complicated three-dimensional structure and the related high resolution requirements for a numerical treatment. In Ref. [11] resistive ballooning modes were studied in general geometry based on the linearized equations of motion of resistive magnetohydrodynamics (RMHD). A multiple length scale expansion technique was used based on a small resistivity and growth rate expansion. RMHD equations computed in Ref. [12] for the Wendelstein 7-X (W7-X) configuration are compared and contrasted to the results with W7-AS using the Correra-Restrepo formulation given in Ref. [11]. In W7-X equilibria, it was shown that the destabilizing effect of resistivity is largely compensated by the stabilizing contribution of plasma compression and this behavior persists up to the ideal marginal limit. The situation is different for W7-AS, where larger resistive effects are observed due to higher resistivity and lower plasma pressure. A general theory applicable to 3-D configurations that avoids the usual restricting assumptions ($\omega \gg \omega_{*e} \gg \omega_\kappa$, zero electron inertia, where ω is the mode frequency, ω_κ is the curvature drift frequency and ω_{*e} is the electron diamagnetic drift frequency) is not available.

In this work, the stability criterion for non-ideal MHD ballooning modes is derived for arbitrary three-dimension ideal MHD stable electron-ion plasmas. In the presence of non-ideal effects, ballooning instabilities can be produced at plasma β levels far below the critical β for ideal ballooning instability. Electron inertia, diamagnetic effects, parallel ion dynamics, transverse particle diffusion and perpendicular gyro-viscous stress terms are included in the calculations. Temperature perturbations and equilibrium temperature gradients are ignored for simplicity. For parameters of interest to the Helically Symmetric Experiment (HSX [15]), characteristic growth rates exceed the electron collision frequency. In this regime, electron inertia effects can dominate plasma resistivity and produce an instability whose growth rate scales with the electromagnetic skin depth.

In this work, a unified theory of RBM and inertial ballooning modes is developed where both the effects of ideal MHD free energy (as measured by the asymptotic matching parameter Δ') and geodesic curvature drives in the non-ideal layer are included in the dispersion relation. This unified theory can be applied to the $k_y \leq 1/\text{cm}$ fluctuations and the anomalous plasma transport observed in HSX near $r/a = 0.7$, where $T_e \simeq 100eV$. Resistive-inertia ballooning mode eigenvalues and eigenfunctions are numerically evaluated for a variety of equilibria including axisymmetric shifted circular geometry ($\hat{s} - \alpha$

model) and 3-D stellarator equilibria.

The organization of this paper is as follows. In Section II, linearized ballooning equations are derived from the Ohm's law, vorticity, continuity and total parallel momentum equations. In Section III, the resistive-inertia MHD (RIMHD), Ideal MHD (IMHD) and drift-resistive-inertia ballooning mode (DRIBM) eigenvalue equations are derived and numerically evaluated in $\hat{s}-\alpha$ geometry. The RIMHD modes in the electrostatic limit are calculated for a quasihelically symmetric stellarator (QHS). The results for a QHS are compared and contrasted with those for a magnetic configuration that spoils the helical symmetry by adding mirror terms to the magnetic spectrum. In Section IV, the shear Alfvén and drift acoustic equations in general 3-D geometry are presented in Hamada coordinates. Section V is devoted to an analytical study of these equations using a multiple length scale expansion technique and a derivation of the dispersion relation. The conclusions are presented in Section VI.

II. Dissipative drift ballooning equations

The reduced Braginskii fluid equations are used for a four-field model of drift resistive ballooning modes. The equations for generalized Ohm's law, vorticity, electron continuity and total momentum can be written following linearized form

$$\mathbf{E}+(\mathbf{v}-\mathbf{j}/en_e)\times\mathbf{B}+\nabla p_e-\eta\mathbf{j}=\frac{m_e}{e^2n_e}\frac{\partial\mathbf{j}}{\partial t}, \tag{1}$$

$$\nabla\cdot n\left(\mathbf{v}_{pi}+\mathbf{v}_{\pi i}\right)+\nabla\cdot n\left(\mathbf{v}_{Di}-\mathbf{v}_{De}\right)+\nabla\cdot\left(n\mathbf{v}_{pe}\right)+\frac{1}{e}\nabla_{\|}\mathbf{j}_{\|}=0, \tag{2}$$

$$\frac{\partial n}{\partial t}+\nabla\cdot n\left(\mathbf{v}_E+\mathbf{v}_{De}\right)+\nabla\cdot n\left(\mathbf{v}_{pe}+\mathbf{v}_{\eta}\right)+\nabla\cdot\left(n\mathbf{v}_{\|e}\right)=0, \tag{3}$$

$$m_in\left(\frac{\partial}{\partial t}+\mathbf{v}_i\cdot\nabla\right)\mathbf{v}_i=-\nabla\left(p_i+p_e\right)+\mathbf{j}\times\mathbf{B}-\nabla\cdot\mathbf{P}_i, \tag{4}$$

where

$$\mathbf{v}_E=-\frac{c}{B}\nabla\phi\times\widehat{\mathbf{b}}, \tag{5}$$

$$\mathbf{v}_{Dj}=-\frac{c}{q_jBn}\nabla p_j\times\widehat{\mathbf{b}}, \tag{6}$$

$$\mathbf{v}_{\pi i}=-\frac{c}{eBn}\nabla\cdot\pi_i\times\widehat{\mathbf{b}}, \tag{7}$$

$$\mathbf{v}_{\eta}=\frac{c}{eBn}\mathbf{R}\times\widehat{\mathbf{b}}, \tag{8}$$

$$\mathbf{v}_{pi}=\frac{1}{\omega_{ci}}\left(\frac{\partial}{\partial t}+\mathbf{v}_i\cdot\nabla\right)\mathbf{v}_i\times\widehat{\mathbf{b}}, \tag{9}$$

and

$$\mathbf{v}_i = \mathbf{v}_E + \mathbf{v}_{Di}. \tag{10}$$

Here $\widehat{\mathbf{b}} = \mathbf{B}/|B|$ is the unit vector along the magnetic field line, $\mathbf{j}_\parallel$ is the plasma current parallel to the magnetic field, ϕ is the electrostatic potential, $P = n(T_i + T_e)$ is the isotropic pressure, π_i is the anisotropic ion stress tensor, and $\mathbf{R}$ denotes the frictional force.

The following expression is obtained by taking the parallel component of Eq. (1) and for simplicity, by assuming uniform temperature along the field line:

$$\mathbf{E}_\parallel + T_e \nabla_\parallel n_e - \eta \mathbf{j}_\parallel = \frac{m_e}{e^2 n_e} \frac{\partial \mathbf{j}_\parallel}{\partial t}, \tag{11}$$

where

$$\mathbf{E}_\parallel = -\nabla_\parallel \phi - \frac{1}{c} \frac{\partial \mathbf{A}_\parallel}{\partial t}, \tag{12}$$

$\nabla_\parallel = \widehat{\mathbf{b}} \cdot \nabla = \widehat{\mathbf{b}}^{(0)} \cdot \nabla + \widehat{\mathbf{b}}^{(1)} \cdot \nabla$, and $\widehat{\mathbf{b}}^{(1)} = \nabla \times \widetilde{\mathbf{A}}_\parallel / B = \nabla \widetilde{\mathbf{A}}_\parallel \times \widehat{e}_\parallel / B$ is the magnetic perturbation associated with field line bending, $A_\parallel$. When quasi-neutrality is assumed, that is, $n = n_e = n_i$, Ampére's law becomes

$$\nabla_\perp^2 \widetilde{\mathbf{A}}_\parallel = -\frac{4\pi}{c} \widetilde{\mathbf{j}}_\parallel. \tag{13}$$

Equations (1)-(4) can be written, using $\partial/\partial t = -i\omega t$, in the following linearized form in $\omega \sim \omega_s \sim \omega_{*j} \sim \omega_\eta$ ordering

$$\left(\omega - \omega_{*en} + \omega H + i c^2 k_\perp^2 \eta_\parallel / 4\pi\right) \widehat{\Psi} = -i c_s \nabla_\parallel \left(\widehat{\Phi} - \widehat{n}\right), \tag{14}$$

$$\omega k_\perp^2 \rho_i^2 \left(\widehat{n} + \tau \widehat{\Phi}\right) = \omega_\kappa \widehat{n} + k_\perp^2 \rho_e^2 \left(\omega - \omega_{*en}\right) \widehat{\Phi} - i \mu_\perp k_\perp^4 \rho_i^2 \left(\widehat{n} + \tau \widehat{\Phi}\right) - i \frac{\tau v_A^2}{c_s} \nabla_\parallel \left(k_\perp^2 \rho_i^2 \widehat{\Psi}\right), \tag{15}$$

$$\omega \widehat{n} - \omega_{*en} \widehat{\Phi} = \omega_{\kappa e} \left(\widehat{\Phi} - \widehat{n}\right) + k_\perp^2 \rho_e^2 \left(\omega - \omega_{*en}\right) \widehat{\Phi} - i c_s \nabla_\parallel \widehat{\mathbf{v}}_\parallel + i \frac{\eta_\perp c^2 k_\perp^2}{4\pi} \frac{c_s^2}{v_A^2} \widehat{n} + i \frac{\tau v_A^2}{c_s} \nabla_\parallel \left(k_\perp^2 \rho_i^2 \widehat{\Psi}\right), \tag{16}$$

$$\left(\omega + \omega_{\kappa i}\right) \widehat{\mathbf{v}}_\parallel + \omega_{*en} \widehat{\Psi} = -i c_s \nabla_\parallel \widehat{n} - 4 i \mu_\perp k_\perp^2 \widehat{v}_\parallel, \tag{17}$$

where $H = k_\perp^2 \delta_e^2$, $\delta_e^2 = c^2/\omega_{pe}^2$, is the electromagnetic skin depth, ω is the mode frequency, $\omega_{pe}^2 = 4\pi n e^2/m_e$ is the electron plasma frequency, $\mu_\perp = 0.3 \nu_i \rho_i^2$ is the classical perpendicular viscosity, $\rho_i = v_{ti}/\omega_{ci}$ is the ion Larmor radius, $v_{ti} = \sqrt{T_i/m_i}$ is the ion thermal velocity, $\omega_{ci} = eB/m_i c$ is the ion cyclotron frequency, $\tau = T_e/T_i$ is the ratio of electron to ion temperature, $v_A^2 = B^2/4\pi n m_i$ is the Alfvén speed, and $\eta_\parallel$ and $\eta_\perp$ are the longitudinal and transverse Spitzer resistivities. Here, $\widehat{\Psi} = e c_s \widetilde{A_\parallel}/c T_e$, $\widehat{\Phi} = e\widetilde{\phi}/T_e$, $\widehat{v}_\parallel = \widetilde{v_\parallel}/c_s$, and $\widehat{n} = \widetilde{n}/n$, are the dimensionless perturbed parallel component of vector potential, electrostatic potential, parallel ion flow and density, respectively. The frequency ω_{*en} in (14) is the diamagnetic drift frequency [$\omega_{*en} = -\left(cT_e/eB\right) \mathbf{k} \cdot \widehat{e}_\parallel \times \nabla \ln n$], and the frequency ω_κ in (15)

is the curvature drift frequency ($\omega_\kappa = \omega_{\kappa i} + \omega_{\kappa e}$) in which $\omega_{\kappa j} = (2cT_j/eB)\,\mathbf{k}\cdot\widehat{e}_\parallel \times \kappa$ and where $c_s = (T_e + T_i/m_i)^{1/2}$ is the sound speed.

III. Ballooning equations in shifted circular geometry

Ballooning modes are a pressure driven instabilities in the presence of finite $k_\parallel$. For the interchange perturbation, the parallel component of the propagation vector is zero ($k_\parallel = 0$), and an average minimum-B condition is stabilizing to the instability. When studying a perturbation in which $k_\parallel \neq 0$ but $k_\parallel/k_\perp \ll 1$, it is possible that one might find that the perturbation can grow locally in the bad curvature region of average minimum-B field. This type of instability is called a ballooning instability. Ballooning instabilities can be resistive or ideal depending upon whether the electron motion parallel to the field is impeded as a result of collisions or inductive fields. For parameters of interest to HSX [15], the characteristic growth rate exceeds the electron collision frequency. Therefore, the electron inertia is included here in the parallel Ohm's law. In this Section, drift-resistive-inertia ballooning (DRIBM), resistive-inertia MHD (RIMHD) and ideal MHD (IMHD), eigenvalue equations are derived after employing the standard high n ballooning mode formalism [13].

The DRIBM equation can be written as follows after ignoring parallel ion momentum, perpendicular viscous stress and the transverse particle diffusion terms in Eqs (14)-(17):

$$\omega_A^2 \frac{d}{d\theta}\left(\frac{k_\perp^2\rho_s^2}{\omega_{Pe}+\omega_R\widehat{k}_\perp^2}\frac{dU}{d\theta}\right) = \frac{\omega_k\left(\omega_{ke}-\omega_{*en}\right)+\left(\omega_k-\omega+\omega_{ki}\right)\omega_{Pi}k_\perp^2\rho_s^2}{\omega_{Pe}+\left(1+1/\tau\right)\omega_{ke}+\omega_{Pi}k_\perp^2\rho_s^2}U, \tag{18}$$

The quantity $U = \Phi - \widehat{n}$ is the non-adiabatic response; $\omega_A = v_A/qR$ is the Alfvén frequency where q is the safety factor and R is the major radius; $k_\perp = (n_\phi q/r)\,\widehat{k}_\perp(\theta)$ where $\widehat{k}_\perp^2(\theta) = 1 + (\hat{s}\theta - \alpha\sin\theta)^2$, $\alpha = -2Rp'q^2/B^2$ is the ballooning parameter, and $\hat{s} = rq'/q$ is the magnetic shear; $\omega_{Pj} = \omega - \omega_{*j}$; $\beta = 8\pi n(T_e+T_i)/B^2$; and $\omega_R = \omega\delta + i\omega_\eta$ where $\delta = c^2k_\theta^2/\omega_{pe}^2$, $\omega_\eta = \left(c^2\eta_\parallel/4\pi\right)(n_\phi q/r)^2$ is the resistive frequency.

The resistive-inertia MHD incompressible ballooning equation (RIMHD) in the high frequency ($|\omega| \gg \omega_{*e}, \omega_{ke}$) long wavelength ($k_\theta^2\rho_i^2 \ll 1$) limit can be written as follows:

$$\omega_A^2 \frac{d}{d\theta}\left(\frac{\widehat{k}_\perp^2}{\omega + (\omega c^2k_\theta^2/\omega_{pe}^2 + i\omega_\eta)\widehat{k}_\perp^2}\frac{d\widehat{\Phi}}{d\theta}\right) + \omega\widehat{k}_\perp^2\widehat{\Phi} + \frac{\omega_{\kappa e}\omega_{*e}}{\omega k_\theta^2\rho_s^2}\left(1+\frac{1}{\tau}\right)\widehat{\Phi} = 0. \tag{19}$$

Note that the electron inertia term, $\omega c^2k_\theta^2/\omega_{pe}^2$, is present in Eqs. (18) and (19). The standard incompressible ideal MHD (IMHD) ballooning equation can be recovered by neglecting electron inertia and

resistivity in the RIMHD equation, Eq. (19),

$$\omega_A^2 \frac{d}{d\theta}\left(\widehat{k}_\perp^2 \frac{d\phi}{d\theta}\right) + \omega^2 \widehat{k}_\perp^2 \phi + \frac{\omega_{\kappa e}\omega_{*i}}{k_\theta^2 \rho_i^2}\left(1+\frac{1}{\tau}\right)\phi = 0, \tag{20}$$

where the usual finite larmor-radius-effect (FLR) (for $k_\perp \rho_i \ll 1$) can be included by substituting $\omega\left(\omega - \omega_{*i}\right)$ for ω^2 in Eq. (20).

IIIa. Numerical results in shifted circular geometry

Equations (18)-(20) are solved numerically by using a standard root finding algorithm for axisymmetric shifted-circle equilibria. (The equilibrium used in obtaining the results shown in Figs. 1-6). For all cases, the parameters used are those appropriate for HSX edge plasmas ($r/a \sim> 0.7$).

Figure 1a shows the normalized growth rate (γ/ω_A) of the IMHD, RIMHD and ideal MHD modes with electron inertia (RIMHD in the limit of $\eta = 0$) as a function of the normalized pressure gradient (the ballooning parameter α), for $\theta_k = 0$, $\hat{s} = 0.1$, $k_\theta \rho = 0.3$, $\hat{\nu} = \nu_e/\omega_A = 0.023$, and $\beta = 0.0002$. In this scan, the positive global magnetic shear $\hat{s} = 0.1$, is chosen to show the ideal MHD unstable region. HSX has reverse shear in the tokamak sense, and the ideal MHD instabilities, for which the mode amplitude does not vary along the field line ($i.e., k_\parallel$=0), are stable for the parameters studied in the limit of perfectly helically symmetric equilibrium. In the presence of 3-D shaping, ideal MHD ballooning instabilities can be excited when $\hat{s} > 0$ [14]. The electron inertia and resistivity result in an instability when the ideal MHD mode is stable. The inertia and resistive modes are purely growing, ($\omega_r = 0$). For HSX-relevant parameters, the electron inertia modes (the RIMHD case for $\eta = 0$) are found to be more important than the resistive modes due to the existence of RIMHD modes in the first ideal stability region. Note that RIMHD modes persist in the ideal MHD second stable regime. Both the electron inertia and resistive instabilities are characterized by broad eigenfunctions along the field lines as shown in Figs. 1a and 1b. The eigenfunctions are found to be relatively strongly localized along field line at higher values of the ballooning parameter α, as shown in the right panel of Fig. 1b. Moreover, the qualitative nature of the eigenfunctions is insensitive to whether or not electron inertia is present. The resistive and electron inertia ballooning eigenfunctions are found to be broad for HSX-relevant values of the ballooning parameter ($\alpha \ll 1$). Therefore, the assumptions $|\omega| \gg \omega_* \gg \omega_{ke}$ and $k_\theta^2 \rho_i^2 \ll 1$ for MHD become suspect and, for a more satisfactory stability analysis, a two fluid formulation is required.

Figure 2 shows the eigenvalues obtained from the drift-resistive-inertia ballooning mode (DRIBM) derived using Eq. (18) in which diamagnetic and first order FLR effects are included. The growth rates of DRIBM are compared with the growth rates of RIMHD modes using the same parameter values as used in Fig. 1, except choosing stellarator-like global shear $\hat{s} = -0.03$ and $k_\theta \rho = 0.1$. The FLR and

diamagnetic effects are found to be slightly stabilizing for RIMHD modes that propagate in the electron diamagnetic flow direction. These stabilizing effects increase the critical α in the first stability region. The RIMHD modes are purely growing (zero real frequency). However, the real frequency of the DRBM mode is shown in the right panel in Fig. 2a. Here, negative values of ω_r indicate mode frequencies in the ion diamagnetic direction. All of these modes are still characterized by broad eigenfunctions in the ballooning space, which indicates an extremely strong radial localization about a mode rational surface, but their width decreases with the increasing ballooning parameter α, as shown in Fig. 2b.

Figure 3a shows the variation of the normalized growth rate and the real frequency as a function of global magnetic shear $\hat{s}$ with $\alpha = 0.1$. The other parameters are the same as in Fig. 2. A reversed magnetic shear (negative value of $\hat{s}$) is found to be more stabilizing than positive magnetic shear because the normal and geodesic curvature in the $g(\theta) = [\cos\theta + (\hat{s}\theta - \alpha\sin\theta)\sin\theta]$ function counteract each other and reduce the destabilizing toroidal effects [4]. The effects of reversed magnetic shear not only reduce the growth rate but, also, extend the eigenfunction along the ballooning angle, as shown in Fig. 3b. HSX has an approximately flat q-profile, low local magnetic shear and unfavorable magnetic curvature at the $\theta_0 = 0 = \zeta_0$ point of the magnetic surface, where θ_0 and ζ_0 are the extended poloidal and toroidal angle like coordinate. Therefore, DRIBMs will be unstable in HSX geometry because these types of modes have large amplitude (balloon) in the region of bad local curvature (for the instability drive) and low local magnetic field shear (to minimize stabilizing effect of field line bending) within each field period, with an envelope that extends over many field periods along field lines.

The growth rate is plotted in Fig. 4 as a function of $k_\theta\rho$ with $\hat{s} = -0.03$ for the RIMHD and DRIBM cases. The other parameters are the same as in Fig. 2. All parts of the k-spectrum are found to be unstable in the incompressible RIMHD model. However, in DRIBM case, the diamagnetic and FLR effects reduce the growth rate and completely stabilize the mode for $k_\theta\rho > 0.2$. Even for $k_\theta\rho \to 0$, the growth rate of DRIBM is found to be smaller than the growth rate of the RIMHD case, which indicates the stabilizing effects of the secularity of the magnetic drift frequency. The real frequency of the DRIBM is found to decrease with increasing $k_\theta\rho$.

Figure 5 shows the dependence of ω on the density scale length $\epsilon_n = L_n/R$ where $L_n = (d_r \ln n)^{-1}$ for $q = 1.0$, $\hat{s} = -0.03$, $\epsilon = 0.0$, $\alpha = 2q^2\beta/\epsilon_n$, $\tau = 1.0$, $\beta = 0.002$, $k_\theta\rho = 0.1$ $\theta_k = 0$, and $\kappa = 1.0$. It is found that as ϵ_n increases, the growth rate decreases, while the real frequency increases. The mode is completely stabilized for $\epsilon_n \leq 0.02$ (for small ϵ_n, $|\omega_\kappa|/\omega \ll 1$ and become negligible) and $\epsilon_n \geq 0.112$ (due to compressibility effects). At low density gradients, growth rates decrease and the eigenfunction becomes broader along the field line is shown in Fig. 5b.

The variation of the growth rate and real frequency is shown in Fig. 6 as a function of β for $k_\theta\rho = 0.01$,

and $\tau = 0.025$, where the other parameters are the same as in Fig. 5. There is no mode threshold at low values of β. However, as β increases, the growth rate and real frequency decrease and the mode becomes completely stabilized at $\beta = 0.17$. This is due to ω_* stabilization at high β. As shown in Fig. 6b, the resistive and inertia effects become unimportant for $\beta \sim 0.17$, and the transition to an ideal mode results under these conditions.

IIIb. Numerical results in an HSX geometry

Equation (19) is solved numerically in the electrostatic limit using three dimensional equilibria for a quasihelically symmetric (QHS) stellarator and a configuration whose ("Mirror") symmetry is spoiled by the presence of magnetic mirror contribution to the magnetic spectrum [15]. The ballooning mode formalism and WKB type boundary conditions [16, 17] are used to solve an eigenvalue problem for the resistive-inertia MHD equation in the electrostatic limit using a fully three-dimensional hydrodynamic equilibria. The equilibria are computed using the VMEC code [18] with fixed boundary conditions for QHS and Mirror mode configurations and for a set of ninety eight magnetic surfaces. The VMEC coordinate system is not a straight field line coordinate system. Thus, before the resistive-inertia MHD ballooning equation is solved in the electrostatic limit, the equilibria is first transformed to Boozer coordinates [19]. Then, the contravariant and covariant basis vectors are constructed for each flux surface and used to calculate the magnetic field, the magnetic field line curvature, the local magnetic shear, and the derivatives of the magnetic field in a fully three dimensional configuration. The details are described in Ref. [20].

Figure 7 contains a plot of the growth rate γ, normalized by R/c_s, as a function of $(k_\perp \rho)^2$ for $\tau = 1$, $R\nu_e/2c_s = 0.42$, $\theta_k = 0.0$, and $\epsilon_n = 0.07$. This calculation is carried out for the field line that intersects the location $\theta_0 = 0$, $\zeta_0 = 0$ on the normalized magnetic surface $s = 0.8980$ as given in [21]. This point is chosen because it is thought to be the most unstable since the local magnetic shear is small, the local value of the geodesic curvature is zero and the destabilizing influence of the normal curvature is strongest. In the left panel of Fig. 7, the bottom curve, denoted with squares, is for the highly resistive case (HR where $\delta = 0$, $\nu_e \neq 0$); the curve, denoted with x's, is for the collisionless case ($\nu_e = 0$, $\delta \neq 0$); and the top curve, denoted with triangles, is for nonzero electron inertia and collisionality (EI+collisions). All three cases are found to be unstable for QHS relevant parameters and their growth rates increase with increasing mode number. The corresponding mode structures are shown in the right panel of Fig. 7 for $(k_\perp \rho)^2 = 0.24$. In comparison with the ion temperature gradient and drift modes calculated in electrostatic limit in our earlier published work [20, 22], these modes are found to be very extended ($\zeta_0 = 20\pi$) along the magnetic field line. However, as the growth rate increases among three cases, the

eigenfunctions become relatively localized.

The highly resistive (HR: $\delta = 0$, $\nu_e \neq 0$) growth rate in QHS is compared with the growth rate for the corresponding Mirror case illustrated in Fig.8. In both configurations, the magnitudes of the linear growth rates are found to be comparable, indicating roughly the same level of anomalous transport flux that is observed in the edge region of experiments. This result is consistent with our earlier findings for ITG and drift modes [20, 22]. The common stability properties are due to the similar structure of the curvature and the local magnetic shear.

IV. Shear-Alfvén and Drift acoustic equation in 3-D geometry

In general, Eqs. (14)-(17) can be reduced to a coupled system of a two second order differential equations, the shear-Alfvén equation and the drift-acoustic equation:

$$\begin{aligned}
&(\mathbf{B}\cdot\nabla)\left[\frac{(\omega-\omega_{*e})\,k_\perp^2\,(\mathbf{e}_\parallel\cdot\nabla)\,U}{B\left(\omega-\omega_{*e}+\omega k_\perp^2\delta_e^2+ic^2k_\perp^2\eta_\parallel/4\pi\right)}\right]+\frac{\omega_\kappa\omega_{*i}}{v_A^2\rho_i^2}\,(U+V)\\
&\quad=-\frac{k_\perp^2}{v_A^2}\left(\omega+i\mu_\perp k_\perp^2\right)\left[(\omega-\omega_{*i})\,U-(1+\tau)\,\omega_{*i}V\right],
\end{aligned}\tag{21}$$

and

$$\begin{aligned}
&\left[(\mathbf{e}_\parallel\cdot\nabla)^2-2\,(\mathbf{e}_\parallel\cdot\nabla)\ln B\,(\mathbf{e}_\parallel\cdot\nabla)\right]V+\frac{(\omega-\omega_{*e})\left(\omega+4i\mu_\perp k_\perp^2\right)}{c_s^2}V\\
&=\left[\frac{\left(\omega+4i\mu_\perp k_\perp^2\right)}{c_s^2}\left(\frac{\omega k_\perp^2\rho_i^2}{\omega_{*i}}-\frac{\omega_{\kappa i}}{\omega_{*i}}\right)+\frac{\left(\omega\delta_e^2+i\eta^*\right)\left(\omega+i\mu_\perp k_\perp^2\right)}{\omega-\omega_{*e}}\frac{k_\perp^2}{v_A^2}\right]\left[(\omega-\omega_{*i})\,U-(1+\tau)\,\omega_{*i}V\right]\\
&+\left[\left(\frac{\omega\delta_e^2+i\eta^*}{\omega-\omega_{*e}}\right)\left(\frac{\omega_\kappa\omega_{*i}}{v_A^2\rho_i^2}\right)-\frac{\eta_\perp}{\eta_\parallel}i\eta^*\left(\omega+4i\mu_\perp k_\perp^2\right)\frac{k_\perp^2}{v_A^2}\right](U+V)+(\mathbf{e}_\parallel\cdot\nabla)\ln\left(\omega+4i\mu_\perp k_\perp^2\right)\\
&\times\left[\frac{\left(\omega\delta_e^2+i\eta^*\right)k_\perp^2}{\omega-\omega_{*e}+\left(\omega\delta_e^2+i\eta^*\right)k_\perp^2}\,(\mathbf{e}_\parallel\cdot\nabla)\,U+(\mathbf{e}_\parallel\cdot\nabla)\,V\right]
\end{aligned}\tag{22}$$

where

$$U=\widehat{\Phi}-\widehat{n},\tag{23}$$

and

$$V=\frac{\omega}{\omega_{*e}}\widehat{n}-\widehat{\Phi}.\tag{24}$$

Unlike the calculations of Section III, here we explicitly keep sound wave physics by allowing non-zero parallel ion dynamics. The equilibrium magnetic field in the Hamada coordinate system (v,θ,ζ) is

$$\mathbf{B}=\nabla v\times\left(\dot{\psi}\nabla\theta-\dot{\chi}\nabla\zeta\right),\tag{25}$$

where v is the volume enclosed within the flux surface, which is used to label the flux surface; θ and ζ are angle-like coordinates that increase by unity after one turn around the torus the short way and the long way, respectively; ψ and χ are flux surface functions corresponding to longitudinal and transverse fluxes respectively. In this notation, a dot over quantities indicates a derivative with respect to the volume. The Hamada coordinate system has a unit Jacobian

$$\nabla v \cdot \nabla\theta \times \nabla\zeta = 1, \tag{26}$$

so that

$$q = \frac{\dot{\psi}}{\dot{\chi}} = \frac{\mathbf{B}\cdot\nabla\zeta}{\mathbf{B}\cdot\nabla\theta} = \frac{d\psi}{d\chi}, \tag{27}$$

is the safety factor. Since magnetic field lines lie on flux surfaces, the contravariant component in the radial direction vanishes: $\mathbf{B}\cdot\nabla v = 0$.

The coordinates $(v, \theta, \varphi = \zeta - q\theta)$ are introduced by transforming $(v,\ \theta,\ \zeta) \rightarrow (v,\ \theta,\ \varphi)$. The transformed basis vectors satisfy

$$\mathbf{B}\cdot\nabla v = 0, \quad \mathbf{B}\cdot\nabla\theta = \dot{\chi}, \quad \mathbf{B}\cdot\nabla\varphi = 0. \tag{28}$$

In this new set of coordinates, there is only one coordinate not orthogonal to $\mathbf{B}$, where

$$\mathbf{B} = \dot{\chi}\nabla\varphi \times \nabla v. \tag{29}$$

Since q=q(v), the property of unit Jacobian is retained:

$$\nabla v \cdot \nabla\theta \times \nabla\varphi = 1. \tag{30}$$

The shear-Alfvén and drift acoustic equations can be expressed by using Hamada coordinates and a ballooning mode formalism:

$$\begin{aligned} & \frac{d}{dy}\left[\frac{(\omega-\omega_{ne})\,K^2 dU/dy}{B^2\left(\omega-\omega_{ne}+\left(\omega\delta_e^2+i\eta^*\right)a^2K^2\right)}\right] + \frac{8\pi\dot{p}\left(\kappa_v+\dot{q}y\kappa_\varphi\right)}{\dot{\chi}^4}\left(U+V\right) \\ = & -\frac{K^2}{\dot{\chi}^2 v_A^2}\left(\omega+i\mu_\perp a^2K^2\right)\left[\left(\omega-\omega_{ni}\right)U-\left(1+\tau\right)\omega_{ni}V\right], \end{aligned} \tag{31}$$

and

$$
\begin{aligned}
&\frac{d}{dy}\left(\frac{\dot{\chi}^2}{B^2}\frac{dV}{dy}\right)+\frac{(\omega-\omega_{ne})\left(\omega+4i\mu_\perp a^2K^2\right)}{c_s^2}V \\
= &\left[-\frac{\left(\omega+4i\mu_\perp a^2K^2\right)}{c_s^2}\left(2L_{nv}\left(\kappa_v+\dot{q}y\kappa_\varphi\right)+\frac{\tau\omega a^2K^2\rho_i^2}{\omega_{ne}}\right)+\frac{\left(\omega\delta_e^2+i\eta^*\right)\left(\omega+i\mu_\perp a^2K^2\right)}{\omega-\omega_{ne}}\frac{a^2K^2}{v_A^2}\right]\times \\
&\left[(\omega-\omega_{ni})U-(1+\tau)\omega_{ni}V\right]+\left[\left(\frac{\omega\delta_e^2+i\eta^*}{\omega-\omega_{ne}}\right)\frac{8\pi a^2\dot{p}\left(\kappa_v+\dot{q}y\kappa_\varphi\right)}{\dot{\chi}^2}-\frac{\eta_\perp}{\eta_\parallel}\frac{i\eta^*\left(\omega+4i\mu_\perp a^2K^2\right)a^2K^2}{v_A^2}\right]\times \\
&(U+V)+\frac{\dot{\chi}^2}{B^2}\frac{d}{dy}\ln\left(\omega+4i\mu_\perp a^2k_\perp^2\right)\left[\frac{\left(\omega\delta_e^2+i\eta^*\right)a^2K^2}{\omega-\omega_{*e}+\left(\omega\delta_e^2+i\eta^*\right)a^2K^2}\frac{dU}{dy}+\frac{dV}{dy}\right], \qquad (32)
\end{aligned}
$$

where

$$
K^2=\left|\nabla\varphi\right|^2-2\dot{q}y\nabla\varphi\cdot\nabla v+\dot{q}^2y^2\left|\nabla v\right|^2, \qquad (33)
$$

$a=\partial S/\partial\varphi$ is the "mode number" that describes the component of the $\mathbf{k}$ vector that is perpendicular to the magnetic field and lies within the magnetic surface; $\eta^*=\left(c^2/4\pi\right)\eta_\parallel$; $p=nT$ is the equilibrium pressure; $L_{nv}\equiv\left(d\ln n/dv\right)^{-1}$; $\kappa_v=\kappa\cdot\nabla\theta\times\nabla\varphi$ is the geodesic curvature; $\kappa_\varphi=\kappa\cdot\nabla v\times\nabla\theta=(-\dot{\chi}/2\dot{p})\mathbf{B}\cdot\nabla\sigma$ is the normal curvature; and $\sigma=\mathbf{j}\cdot\mathbf{B}/B^2$. The coordinate y is defined as labeling points along the magnetic field and, as such, $\mathbf{B}\cdot\nabla=\dot{\chi}(d/dy)$.

V. Analysis of Resistive Ballooning Mode equations

Analytic progress can be made toward understanding the structure of non-ideal MHD ballooning modes by using a multiple scale analysis. This derivation generalizes the work of Hastie *et al.* [6] to three-dimensional equilibria. A small parameter ϵ can be defined that accounts for the disparate timescales associated with current diffusion time and the Alfvén time.

$$
\epsilon\equiv\left(\frac{\omega_\eta}{\omega_A}\right)^{1/3}\ll 1, \qquad (34)
$$

In the following derivation, a somewhat general ordering is used

$$
\omega\sim\omega_s\sim\omega_{nj}\sim\epsilon\omega_A \qquad (35)
$$

and viscosity is assumed to be comparable to resistivity, $\omega_\mu=\epsilon^3\omega_A$. Eqs. (31) and (32) can be solved using a two variable expansion procedure. The variables y and $z=\epsilon y$ are taken as two different length

scales along the magnetic field and the Ansatz used is

$$U\left(y\right)=U_{0}\left(y,z\right)+\epsilon U_{1}\left(y,z\right)+\epsilon^{2}U_{2}\left(y,z\right)+.... \tag{36}$$

and

$$V\left(y\right)=V_{0}\left(y,z\right)+\epsilon V_{1}\left(y,z\right)+\epsilon^{2}V_{2}\left(y,z\right)+.... \tag{37}$$

$$\frac{dU}{dy}=\frac{\partial U}{\partial y}+\epsilon\frac{\partial U}{\partial z} \tag{38}$$

$$U_{i}(y+N,z)=U_{i}(y,z),\quad i=0,1,2,... \tag{39}$$

is used.

The function U depends upon the variable y that characterizes the variation of equilibrium quantities within a flux surface. The variable z accounts for the long envelope of the eigenfunction along the magnetic field line due to non-ideal MHD effects. For $|y|\sim 1$, an ideal MHD region can be identified where resistivity, electron inertia and viscosity can be neglected. The drift acoustic and shear Alfvén equations in the zeroth order in ϵ can be written as

$$\frac{d}{dy}\left(\frac{\dot{\chi}^{2}}{B^{2}}\frac{dV_{0}}{dy}\right)+\frac{\omega\left(\omega-\omega_{ne}\right)}{c_{s}^{2}}V_{0}=0 \tag{40}$$

and

$$\frac{d}{dy}\left[\frac{K^{2}}{B^{2}}\frac{dU_{0}}{dy}\right]+\frac{4\pi}{\dot{\chi}^{4}}\left(2\dot{p}\kappa_{v}-\dot{q}\dot{\chi}^{2}y\frac{d\sigma}{dy}\right)U_{0}=0. \tag{41}$$

In the limit of large values of $|y|$, the shear Alfvén equation yields the following asymptotic solution

$$U=a_{1}\left|y\right|^{s}+a_{2}\left|y\right|^{-1-s},\quad |y|\rightarrow\infty, \tag{42}$$

where

$$s=-\frac{1}{2}+\left[\frac{1}{4}-E-F-H\right]^{1/2}. \tag{43}$$

The quantities E, F and H depend on the equilibrium and are defined as [10]:

$$E=\frac{A\langle B^{2}/\left|\widehat{\nabla}v\right|^{2}\rangle}{\dot{q}^{2}\dot{\chi}^{4}}\left[\dot{I}\ddot{\Psi}-\dot{J}\ddot{\chi}-\dot{q}\dot{\chi}^{2}\frac{\langle\sigma B^{2}\rangle}{\langle B^{2}\rangle}\right]. \tag{44}$$

$$F=\frac{A^{2}\langle B^{2}/\left|\widehat{\nabla}v\right|^{2}\rangle}{\dot{q}^{2}\dot{\chi}^{4}}\left[\langle\frac{B^{2}\sigma^{2}}{\left|\widehat{\nabla}v\right|^{2}}\rangle-\frac{\langle\sigma B^{2}/\left|\widehat{\nabla}v\right|^{2}\rangle^{2}}{\langle B^{2}/\left|\widehat{\nabla}v\right|^{2}\rangle}+\dot{p}^{2}\langle\frac{1}{B^{2}}\rangle\right], \tag{45}$$

$$H = \frac{A^2 \langle B^2 / \left| \widehat{\nabla} v \right|^2 \rangle}{\dot{q} \dot{\chi}^2} \left[\frac{\langle \sigma B^2 \rangle}{\langle B^2 \rangle} - \frac{\langle \sigma B^2 / \left| \widehat{\nabla} v \right|^2 \rangle}{\langle B^2 / \left| \widehat{\nabla} v \right|^2 \rangle} \right], \tag{46}$$

$$D_R = F + E + H^2, \tag{47}$$

Since ideal MHD stability is assumed in this analysis, the Mercier stability criterion is satisfied

$$-D_I = \frac{1}{4} - (E + F + H) = \frac{1}{4} + H^2 - H - D_R \geqq 0. \tag{48}$$

For the solution in the outer region along the field lines ($|y| \gtrsim \epsilon^{-1}$), resistivity, inertia and viscosity must be taken into account. The shear-Alfvén wave equation in the lowest order in ϵ can be written as

$$\frac{d}{dy} \left[\frac{1}{B^2 \left(1 + \widehat{\omega}_{IR}\right)} \frac{dU_0}{dy} \right] = 0, \tag{49}$$

whose solution is $U_0 = U_0(z)$. Thus, U_0 does not explicitly depend on y in this case. In first order, it follows, with the use of Eq. (39), that

$$\begin{aligned} U_1(y,z) &= U_1(z) + A_1 U_0(z) \left[\int \left(\frac{\widetilde{\sigma B^2}}{\left| \widehat{\nabla} v \right|^2} \right) dy + \dot{q}^2 z^2 \widehat{\omega}_{IR} \int \widetilde{\sigma B^2} dy \right] \\ &\quad + A_2(z) \left[\frac{1}{\dot{q}^2 z^2} \int \frac{\widetilde{B^2}}{\left| \widehat{\nabla} v \right|^2} dy + \widehat{\omega}_{IR} \int \widetilde{B^2} dy \right], \end{aligned} \tag{50}$$

where

$$A = 4\pi \left(\overline{a}/q\right)^2, \quad A_1 = \left(\frac{A}{\dot{q} z \dot{\chi}^2} \right), \quad A_2(z) = \frac{L}{M}, \quad \widehat{\omega}_{IR} = \frac{\widehat{\omega} \delta^2 / \epsilon^2 + i}{\widehat{\omega} - \widehat{\omega}_{\ ne}}$$

$$L = \left[\frac{\partial U_0}{\partial z} - A_1 \left(\left\langle \frac{\sigma B^2}{\left| \widehat{\nabla} v \right|^2} \right\rangle - \dot{q}^2 \ z^2 \widehat{\omega}_{IR} \left\langle \sigma B^2 \right\rangle \right) \right], \tag{51}$$

$$M = \frac{1}{\dot{q}^2 \ z^2} \left\langle \frac{B^2}{\left| \widehat{\nabla} v \right|^2} \right\rangle + \widehat{\omega}_{IR} \left\langle B^2 \right\rangle. \tag{52}$$

$$\left\langle B^2 \right\rangle = \left\langle B^2 \right\rangle (v_0, \varphi_0) = \frac{\oint B^2 dy}{\oint dy} \tag{53}$$

$$\widetilde{B^2} = B^2 - \left\langle B^2 \right\rangle, \quad i.e., \quad \left\langle \widetilde{B^2} \right\rangle = 0. \tag{54}$$

and

$$\begin{aligned}
\delta &= \frac{q}{\overline{a}}\left(\frac{c}{\omega_{pe}}\right)\left(\frac{\partial S}{\partial\varphi}\right), \quad \omega_\eta = \frac{c^2\eta_\parallel}{4\pi}\left(\frac{q}{\overline{a}}\right)^2\left(\frac{\partial S}{\partial\varphi}\right)^2, \quad \widehat{\nabla} = \frac{\overline{a}}{q}\nabla, \\
\widehat{\omega} &= \frac{\omega}{\epsilon\omega_A}, \quad \omega_A = \frac{V_A}{L_\parallel}, \quad L_\parallel = 2\pi q R_0, \quad R_0 \equiv \frac{\left\langle B^2\right\rangle^{1/2}}{2\pi q\left|\dot{\chi}\right|} = \frac{\left\langle B^2\right\rangle^{1/2}}{2\pi q\left|\dot{\psi}\right|}.
\end{aligned} \tag{55}$$

In second order, a solubility condition for U_2 is derived by taking into account Eq. (39). The result is a differential equation for U_0 that depends upon integrals of U_1 and V_1:

$$\begin{aligned}
&\left\langle \frac{\partial}{\partial z}\frac{\dot{q}^2z^2\left|\widehat{\nabla}v\right|^2}{B^2A_3}\frac{\partial U_1}{\partial y}\right\rangle = -\frac{A_1\dot{q}zU_0}{\dot{\chi}^2}\left[\langle 2\dot{p}\kappa_v\rangle - \dot{q}z\dot{\chi}^2\left(\left\langle\frac{\partial\sigma}{\partial z}\right\rangle - \left\langle\left(\frac{\partial U_1}{\partial y}+\frac{\partial V_1}{\partial y}\right)\sigma\right\rangle\right)\right] \\
&-\left\langle \frac{\partial}{\partial z}\frac{\dot{q}^2z^2\left|\widehat{\nabla}v\right|^2}{B^2A_3}\frac{\partial U_0}{\partial z}\right\rangle - \dot{q}^2\ z^2\left(\widehat{\omega}-\widehat{\omega}_{\ ni}\right)U_0\left\langle\frac{\left|\widehat{\nabla}v\right|^2}{B^2}\left(\widehat{\omega}+i\,\widehat{\mu}\dot{q}^2z^2\ \left|\widehat{\nabla}v\right|^2\right)\right\rangle,
\end{aligned} \tag{56}$$

where $A_3 = 1+\dot{q}^2z^2\widehat{\omega}_{IR}\left|\widehat{\nabla}v\right|^2$.

One special limit that can be pursued analytically is the electrostatic limit. In this case, $\dot{q}^2z^2\widehat{\omega}_{IR}\left|\widehat{\nabla}v\right|^2 \gg 1$, and $V_1 = 0$ yields

$$\frac{d^2U_0}{dz^2} + W_1\left[\langle 2\dot{p}\kappa_v\rangle + \dot{q}\dot{\chi}^2\left(\langle\sigma\rangle - \frac{\langle\sigma B^2\rangle}{\langle B^2\rangle}\right)\right]U_0 + W_2\left[\left\langle\sigma^2B^2\right\rangle - \frac{\left\langle\sigma B^2\right\rangle^2}{\langle B^2\rangle} - W_3\left\langle\frac{\left|\widehat{\nabla}v\right|^2}{B^2}\right\rangle\right]z^2U_0 = 0, \tag{57}$$

where

$$W_1 = \left(\frac{A}{\dot{\chi}^4}\right)\widehat{\omega}_{IR}\left\langle B^2\right\rangle, \quad W_2 = \frac{\dot{q}^2\dot{\chi}^4}{\langle B^2\rangle}W_1^2, \quad W_3 = \widehat{\omega}\left(\widehat{\omega}-\widehat{\omega}_{ni}\right)\frac{\dot{q}^2\left\langle B^2\right\rangle}{W_2}. \tag{58}$$

The condition for existence of a solution is $2\dot{p}\left\langle\kappa_v\right\rangle + \dot{q}^2\dot{\chi}^2\left(\langle\sigma\rangle - \left\langle\sigma B^2\right\rangle/\left\langle B^2\right\rangle\right) > 0$. The solutions of Eq. (57) in this case result in the following eigenvalue expression

$$U_{0n} = \exp\left(-z_1^2\right)H_n\left(z_1\right), \tag{59}$$

where

$$z_1^2 = \left[W_2\left(\frac{\left\langle\sigma B^2\right\rangle^2}{\langle B^2\rangle} - \left\langle\sigma^2B^2\right\rangle - W_3\left\langle\frac{\left|\widehat{\nabla}v\right|^2}{B^2}\right\rangle\right)\right]z^2, \tag{60}$$

and where H_n are Hermite polynomials of order n. The resulting dispersion relation is

$$\begin{aligned}\omega\left(\omega-\omega_{ne}\right)\left(\omega-\omega_{ni}\right) &= -\frac{\omega_A^2\left(\omega\delta^2+i\omega_\eta\right)}{\left\langle\left|\widehat{\nabla}v\right|^2/B^2\right\rangle}\left(\frac{4\pi\left(\overline{a}/q\right)^2}{\dot{\chi}^2}\right)^2\left[\left\langle\sigma^2B^2\right\rangle-\left\langle\sigma B^2\right\rangle^2/\left\langle B^2\right\rangle\right.\\ &\left.+\frac{\left\langle B^2\right\rangle}{\left(\dot{q}^2\dot{\chi}^4\left(2n+1\right)^2\right)}\times\left\{\left\langle 2\dot{p}\kappa_v\right\rangle+\dot{q}\dot{\chi}^2\left(\left\langle\sigma\right\rangle-\frac{\left\langle\sigma B^2\right\rangle}{\left\langle B^2\right\rangle}\right)\right\}^2\right]. \qquad (61)\end{aligned}$$

Solutions to this dispersion relation lead to an infinite sequence of modes with growth rates scaling as the resistive ballooning mode, $\gamma\sim{\omega_\eta}^{1/3}$, or the electron inertia ballooning mode, $\gamma\sim\delta$. In the absence of drift effects, the modes are purely growing, as can also be seen in the numerical results reported in Section III.

a) Coupling of visco-resistive ballooning modes to drift-acoustic waves

When the value of U_1 from Eq. (50) is used in the solubility equation (56), one obtains the following equation in the $\omega\sim\omega_s$ ordering:

$$\begin{aligned}&\frac{\partial}{\partial X}\frac{X^2}{1+X^2}\frac{\partial U_0}{\partial X}+\frac{H\left(1-H\right)}{\left(1+X^2\right)^2}\left(U_0+V_0\right)-\frac{H\left(1+H\right)X^2}{\left(1+X^2\right)^2}\left(U_0+V_0\right)+D_R\left(U_0+V_0\right)-\left(Q_3V_0+Q_1U_0\right)X^2\\ =\;&\left(Q_2U_0+Q_4V_0\right)X^4-\frac{AN_1X}{\dot{q}\dot{\chi}^2}\left[\left\langle\frac{\sigma}{\sqrt{o_1}}\frac{\partial V_1}{\partial y}\right\rangle+\left\langle\sigma\right\rangle\frac{\partial V_0}{\partial X}-\frac{M_1}{N_1\left(1+X^2\right)}\frac{\partial V_0}{\partial X}\right], \qquad (62)\end{aligned}$$

where

$$\begin{aligned}\frac{\partial}{\partial y}\frac{1}{B^2}\frac{\partial V_1}{\partial y} &= -\frac{\left(\widehat{\omega}-\widehat{\omega}_{ne}\right)\left(\widehat{\omega}+4i\widehat{\mu}_\perp\dot{q}^2z^2\left|\widehat{\nabla}v\right|^2\right)}{\left\langle B^2\right\rangle\widehat{\omega}_s^2}V_1\left(y,z\right)+\dot{q}z\frac{d\sigma}{dy}\left[\frac{\dot{\chi}^2}{4\pi\dot{p}^2}\left(\widehat{\omega}+4i\widehat{\mu}_\perp\dot{q}^2z^2\left|\widehat{\nabla}v\right|^2\right)\right.\\ &\left.\times\left(\widehat{\omega}-\widehat{\omega}_{ni}\right)-\frac{A\widehat{\omega}_{IR}}{\dot{\chi}^2}\right]U_0, \qquad (63)\end{aligned}$$

$$Q_1=-\frac{A^2N_1^2}{\dot{q}^2\dot{\chi}^4\left\langle B^2\right\rangle}\left[\frac{\dot{q}}{A}\frac{\omega\left(\omega-\omega_{ni}\right)\left(\omega-\omega_{ne}\right)}{\omega_A^2\left(\omega\delta^2+i\omega_\eta\right)}\left(\frac{1}{A}\left\langle\frac{\left|\widehat{\nabla}v\right|^2}{B^2}\right\rangle\right)+I\right],\quad I=\left\langle\sigma^2B^2\right\rangle-\frac{\left\langle\sigma B^2\right\rangle^2}{\left\langle B^2\right\rangle}, \qquad (64)$$

$$Q_2=-\frac{i\omega_\mu\left(\omega-\omega_{ni}\right)\left(\omega-\omega_{ne}\right)^2N_1^3}{\dot{q}^2\left\langle B^2\right\rangle\omega_A^2\left(\omega\delta^2+i\omega_\eta\right)^2}\left\langle\frac{\left|\widehat{\nabla}v\right|^2}{B^2}\right\rangle^2,\quad N_1=\left\langle\frac{B^2}{\left|\widehat{\nabla}v\right|^2}\right\rangle,\quad o_1=\frac{\dot{q}^2\left\langle B^2\right\rangle}{N_1}\widehat{\omega}_{IR}, \qquad (65)$$

$$Q_3=\frac{A^2N_1^2}{\dot{q}^2\dot{\chi}^4\left\langle B^2\right\rangle}\left[\frac{\dot{\chi}^4}{A}\frac{\omega\left(1+\tau\right)\omega_{ni}\left(\omega-\omega_{ne}\right)}{\omega_A^2\left(\omega\delta^2+i\omega_\eta\right)}\left(\frac{1}{A}\left\langle\frac{\left|\widehat{\nabla}v\right|^2}{B^2}\right\rangle\right)-I\right], \qquad (66)$$

and

$$Q_4 = \frac{i\omega_\mu \left(1+\tau\right)\omega_{ni}\left(\omega-\omega_{ne}\right)^2 N_1^3}{\dot{q}^2\left\langle B^2\right\rangle \omega_A^2\left(\omega\delta^2+i\omega_\eta\right)^2}\left\langle \frac{\left|\widehat{\nabla}v\right|^2}{B^2}\right\rangle^2, \quad M_1 = \left\langle \frac{\sigma B^2}{\left|\widehat{\nabla}v\right|^2}\right\rangle + N_1\frac{\left\langle\sigma B^2\right\rangle}{\left\langle B^2\right\rangle}X^2. \tag{67}$$

Assuming $\mu = 0$ and $\sigma \propto \sin(M-Nq)y$, where M is the poloidal mode number and N is the toroidal mode number(the number of field periods). Then, the solubility condition for U_2 given in Eq. (62), takes the following form:

$$\frac{\partial}{\partial X}\frac{X^2}{1+X^2}\frac{\partial U_0}{\partial X} + \frac{H\left(1-H\right)}{\left(1+X^2\right)^2}U_0 - \frac{H\left(1+H\right)X^2}{\left(1+X^2\right)^2}U_0 + D_R U_0 - Q_{1V}U_0X^2 = 0, \tag{68}$$

where

$$Q_{1V} = -\frac{A^2N_1^2}{\dot{q}^2\dot{\chi}^4\left\langle B^2\right\rangle}\left[\frac{\dot{\chi}^4}{A}\frac{\omega\left(\omega-\omega_{ni}\right)\left(\omega-\omega_{ne}\right)}{\omega_A^2\left(\omega\delta^2+i\omega_\eta\right)}\left(\frac{1}{A}\left\langle\frac{\left|\widehat{\nabla}v\right|^2}{B^2}\right\rangle + P_S\frac{\left\langle\sigma^2B^2\right\rangle}{4\pi\dot{p}^2}\right) + \left\langle\sigma^2B^2\right\rangle\left(1-P_S\right) - \frac{\left\langle\sigma B^2\right\rangle^2}{\left\langle B^2\right\rangle}\right], \tag{69}$$

and

$$P_S = \frac{(M-Nq)\omega_s^2}{(M-Nq)^2\omega_s^2 - \omega\left(\omega-\omega_{ne}\right)}. \tag{70}$$

Equation (68) describes the coupling between the drift resistive ballooning mode and the drift acoustic mode in the limit that the mode frequency is comparable to the sound wave frequency.

If the frequency of the mode is assumed to be smaller than the sound frequency ($\omega_s \gg \omega$), then $V_0\left(z\right) \neq 0$, and Eq. (63) can be written as

$$\begin{aligned} V_1 \;=\; & \frac{\partial V_0}{\partial z}\frac{\int\widetilde{B^2}dy}{\left\langle B^2\right\rangle} + \dot{q}\dot{\chi}^2 z\left[\frac{\widehat{\omega}\left(\widehat{\omega}-\widehat{\omega}_{ni}\right)U_0 - \left(1+\tau\right)\widehat{\omega}\widehat{\omega}_{ni}V_0}{4\pi\dot{p}^2} - \frac{A\widehat{\omega}_{IR}\left(U_0+V_0\right)}{\dot{\chi}^4}\right]\left[\int\widetilde{\sigma B^2} - \frac{\left\langle\sigma B^2\right\rangle}{\left\langle B^2\right\rangle}\int\widetilde{B^2}\right]dy \\ & 4i\widehat{\mu}\dot{q}^2z^2\left[\left(\widehat{\omega}-\widehat{\omega}_{ni}\right)U_0 - \left(1+\tau\right)\widehat{\omega}_{ni}V_0\right]\left[\int\widetilde{\left|\widehat{\nabla}v\right|^2\sigma B^2} - \frac{\left\langle\left|\widehat{\nabla}v\right|^2\sigma B^2\right\rangle}{\left\langle B^2\right\rangle}\int\widetilde{B^2}\right]dy + V_1\left(z\right), \end{aligned} \tag{71}$$

The following second order differential equation for the shear Alfvén mode is derived by using V_1 in Eq. (62):

$$\begin{aligned} & \frac{\partial}{\partial X}\frac{X^2}{1+X^2}\frac{\partial U_0}{\partial X} + \frac{H\left(1-H\right)}{\left(1+X^2\right)^2}\left(U_0+V_0\right) - \frac{H\left(1+H\right)X^2}{\left(1+X^2\right)^2}\left(U_0+V_0\right) + \frac{HX}{1+X^2}\frac{\partial V_0}{\partial X} + D_R\left(U_0+V_0\right) \\ = \;& \left(Q_{1M}U_0 + Q_{3M}V_0\right)X^2 + \left(Q_{2M}U_0 + Q_{4M}V_0\right)X^4. \end{aligned} \tag{72}$$

Similarly, a solubility equation for V_2 can be obtained for drift acoustic mode

$$\begin{aligned}
&\frac{\partial^2 V_0}{\partial X^2}+\left(1+Q_*\right)\frac{H^2}{1+X^2}V_0+\left(Q_*+\frac{\Omega\dot{\chi}^4}{A4\pi\dot{p}^2}\right)\left[\frac{H^2X^2}{1+X^2}+\frac{A^2N_1}{\dot{q}^2\dot{\chi}^4}I_2\right]V_0+\left(Q_5U_0-Q_6V_0\right)X^2\\
=\;&\left(1+Q_*\right)D_RV_0+\left(1-\frac{\Omega\dot{\chi}^4}{A4\pi\dot{p}^2}\right)\left[D_R-\frac{H^2}{1+X^2}-\frac{HX}{1+X^2}\frac{\partial}{\partial X}\right]U_0,
\end{aligned}\tag{73}$$

where $Q_1$to Q_4 in Eqs. 64 to 67 are modified as follows:

$$Q_{1M}=-\frac{A^2N_1^2}{\dot{q}^2\dot{\chi}^4\left\langle B^2\right\rangle}\left[\frac{\dot{\chi}^4}{A}\frac{\omega\left(\omega-\omega_{ni}\right)\left(\omega-\omega_{ne}\right)}{\omega_A^2\left(\omega\delta^2+i\omega_\eta\right)}\left(\frac{1}{A}\left\langle\frac{\left|\widehat{\nabla}v\right|^2}{B^2}\right\rangle+\frac{I}{4\pi\dot{p}^2}\right)\right],\tag{74}$$

$$Q_{2M}=-\frac{i\omega_\mu\left(\omega-\omega_{ni}\right)\left(\omega-\omega_{ne}\right)^2N_1^3}{\dot{q}^2\left\langle B^2\right\rangle\omega_A^2\left(\omega\delta^2+i\omega_\eta\right)^2}\left[\left\langle\frac{\left|\widehat{\nabla}v\right|^2}{B^2}\right\rangle^2+\frac{AI_1}{\pi\dot{p}^2}\right],\tag{75}$$

$$Q_{3M}=\frac{A^2N_1^2}{\dot{q}^2\dot{\chi}^4\left\langle B^2\right\rangle}\left[\frac{\dot{\chi}^4}{A}\frac{\omega\left(1+\tau\right)\omega_{ni}\left(\omega-\omega_{ne}\right)}{\omega_A^2\left(\omega\delta^2+i\omega_\eta\right)}\left(\frac{1}{A}\left\langle\frac{\left|\widehat{\nabla}v\right|^2}{B^2}\right\rangle+\frac{I}{4\pi\dot{p}^2}\right)\right],\tag{76}$$

$$Q_{4M}=\frac{i\omega_\mu\left(1+\tau\right)\omega_{ni}\left(\omega-\omega_{ne}\right)^2N_1^3}{\dot{q}^2\left\langle B^2\right\rangle\omega_A^2\left(\omega\delta^2+i\omega_\eta\right)^2}\left[\left\langle\frac{\left|\widehat{\nabla}v\right|^2}{B^2}\right\rangle^2+\frac{AI_1}{\pi\dot{p}^2}\right],\tag{77}$$

$$Q_5=\frac{A^2N_1^2}{\dot{q}^2\dot{\chi}^4\left\langle B^2\right\rangle}\left[\frac{\dot{\chi}^4}{A}\left\{\left(1+a^2Q_*\right)\Omega-i\frac{\eta_\perp}{\eta_\parallel}\frac{\omega\omega_\eta\left(\omega-\omega_{ne}\right)^2}{\omega_A^2\left(\omega\delta^2+i\omega_\eta\right)^2}\right\}\frac{1}{A}\left\langle\frac{\left|\widehat{\nabla}v\right|^2}{B^2}\right\rangle-Q_*\left(1-\frac{\Omega\dot{\chi}^4}{A4\pi\dot{p}^2}\right)I\right],\tag{78}$$

$$Q_6=\frac{A^2N_1^2}{\dot{q}^2\dot{\chi}^4\left\langle B^2\right\rangle}\left[\frac{\dot{\chi}^4}{A}\left\{\left(1+a^2Q_*\right)Q_*+i\frac{\eta_\perp}{\eta_\parallel}\frac{\omega\omega_\eta\left(\omega-\omega_{ne}\right)^2}{\omega_A^2\left(\omega\delta^2+i\omega_\eta\right)^2}\right\}\frac{1}{A}\left\langle\frac{\left|\widehat{\nabla}v\right|^2}{B^2}\right\rangle+\left\{Q_*(Q_*+2)+\frac{\Omega\dot{\chi}^4}{A4\pi\dot{p}^2}\right\}I\right],\tag{79}$$

$$I_1=\frac{\left\langle\left|\widehat{\nabla}v\right|^2\sigma^2B^2\right\rangle}{\left\langle B^2\right\rangle}-\frac{\left\langle\sigma B^2\right\rangle\left\langle\left|\widehat{\nabla}v\right|^2\sigma B^2\right\rangle}{\left\langle B^2\right\rangle^2},\qquad I_2=\left\langle\frac{B^2\sigma^2}{\left|\nabla v\right|^2}\right\rangle-\frac{\left\langle\sigma B^2/\left|\nabla v\right|^2\right\rangle^2}{\left\langle B^2/\left|\nabla v\right|^2\right\rangle},\tag{80}$$

and

$$Q_*=\frac{\left(1+\tau\right)\omega\omega_{ni}\left(\omega-\omega_{ne}\right)}{\omega_A^2\left(\omega\delta^2+i\omega_\eta\right)}\frac{\dot{\chi}^4}{A4\pi\dot{p}^2},\qquad\Omega=\frac{\omega\left(\omega-\omega_{ni}\right)\left(\omega-\omega_{ne}\right)}{\omega_A^2\left(\omega\delta^2+i\omega_\eta\right)}.\tag{81}$$

Equations. (72)-(73) are a fourth order coupled set of flux surface averaged differential equations with the effects of electron-inertia, drifts, viscosity and transverse particle diffusion included . These effects do not appear in Ref. [11]. These equations provide coupling between visco-resistive ballooning modes and drift acoustic waves in the limit where the mode frequency is much smaller than the sound wave

frequency ($\omega_s \gg \omega$).

b) Visco-resistive-inertia ballooning modes

In the limit $\omega \gg \omega_s$, $V_0 = V_1 = 0$, sound wave propagation is neglected and the visco-resistive-inertia ballooning mode equation can be shown to be

$$\frac{\partial}{\partial X}\frac{X^2}{1+X^2}\frac{\partial U_0}{\partial X} + \frac{H\left(1-H\right)}{\left(1+X^2\right)^2}U_0 - \frac{H\left(1+H\right)X^2}{\left(1+X^2\right)^2}U_0 + D_R U_0 - Q_1 U_0 X^2 - Q_2 U_0 X^4 = 0 \tag{82}$$

The limit of zero viscosity, $\omega_\mu = 0$, implies $Q_2 = 0$ in Eq. (82), and the drift-resistive-inertia ballooning equation is recovered. This equation has the same form as the resistive MHD case considered in Ref. [11] except for the diamagnetic and electron inertia corrections that appear in the coefficients Q_1 and Q_0 [defined in Eq. (84) below]. A valid solution can be constructed in the ideal and resistive regions by matching the ideal solution for $|y| \longrightarrow \infty$ to the resistive solution for $|X| \longrightarrow 0$. The resulting general dispersion relation, $\Delta = \Delta'$, is obtained, where Δ' can be calculated by using the conventional definition as the ratio of coefficients of the large and small solutions of the asymptotic form of the ideal solution, which in this case defined as $\Delta' \equiv a_2/a_1$. The expression for Δ is

$$\Delta \equiv \frac{4y_0^{1+2s}Q^{(5-2s)/4}}{Q_1 - \left(1+s-H\right)^2}\frac{\Gamma\left[1/2+s\right]}{\Gamma\left[-1/2-s\right]}\frac{\Gamma\left[\left(1/4\right)\left(Q_1^{1/2}+3-2s-D_R/Q_1^{1/2}\right)\right]}{\Gamma\left[\left(1/4\right)\left(Q_1^{1/2}+1+2s-D_R/Q_1^{1/2}\right)\right]}, \tag{83}$$

where

$$Q_1 = \frac{\omega\left(\omega-\omega_{ni}\right)\left(\omega-\omega_{ne}\right)}{Q_0}, \quad Q_0 = \frac{\dot{q}^2\left\langle B^2\right\rangle\omega_A^2\left(\omega\delta^2+i\omega_\eta\right)}{AN_1M}, \tag{84}$$

$$X^2 = \frac{\dot{q}^2\left\langle B^2\right\rangle\left(\omega\delta^2+i\omega_\eta\right)}{N_1\left(\omega-\omega_{ne}\right)}Z^2 = \frac{Z^2}{y_0^2Q_1}, \quad y_0^2 = \frac{\omega_A^2}{AM\omega\left(\omega-\omega_{ni}\right)}, \tag{85}$$

$$M = \left\langle\frac{B^2}{\left|\widehat{\nabla}v\right|^2}\right\rangle\left[\left\langle\left|\widehat{\nabla}v\right|^2/B^2\right\rangle + \frac{1}{\dot{\chi}^4}\left\{\left\langle\sigma^2B^2\right\rangle - \frac{\left\langle\sigma B^2\right\rangle^2}{\left\langle B^2\right\rangle}\right\}\right], \tag{86}$$

in which Γ is the gamma function. For the special case when $D_R > 0$, this derivation reproduces the stability criterion derived in Ref. [11] with electron inertia and diamagnetic corrections:

$$\omega\left(\omega-\omega_{ne}\right)\left(\omega-\omega_{ni}\right) = -\frac{\omega_A^2\left(\omega\delta^2+i\omega_\eta\right)}{AN_1M}\dot{q}^2\left\langle B^2\right\rangle\left[\left\{\left(\frac{1}{2}+s+2n\right)^2+D_R\right\}^{1/2} - \left(\frac{1}{2}+s+2n\right)\right]^2 \tag{87}$$

In the absence of electron inertia and diamagnetic effects, resistive ballooning modes are found with a growth rate proportional to the the cube root of the resistivity.

VI. Conclusions

A unified theory of resistive and electron inertia ballooning modes has been developed. The drift-resistive-inertia ballooning mode (DRIBM) is characterized by eigenfunctions that are extended along the field line in ballooning space. The qualitative nature of the eigenfunctions is found to be insensitive to whether or not electron inertia is present. However, the resistive and inertia effects become unimportant as the plasma β is increased close to the transition to an ideal mode. Resistive-inertia MHD ballooning modes in the electrostatic limit have large growth rates for large values of $k_\perp \rho_s$ (but still small compared to unity). In the absence of drift effects, the modes are purely growing and they persist in regimes where ideal MHD ballooning modes are stable. These characteristics are also found in three-dimensional analytical calculations. For parameters of interest to HSX, electron inertia effects are more important than plasma resistivity. Electron inertia modes are the most unstable modes and have growth rates that scale with the electron skin depth, $\gamma \sim c/\omega_{pe}$. The magnitudes of the linear growth rates are not sensitive to the magnetic configuration in HSX plasmas. This result would indicate a comparable level of anomalous transport in QHS and mirror configurations, which is consistent with experimental observations in the HSX edge region. The common stability properties in these two configurations are due to a similar structure of the curvature and local magnetic shear. Finally, analytic models for the coupling of visco-resistive ballooning modes to drift acoustic waves are developed in the limits of large and small sound wave frequency compared with the mode frequency.

Acknowledgments

This research was supported by the U.S. DoE under Grants Nos. DE-FG02-99E54546, DE-FG02-86ER53218 and DE-FG02-92ER54141.

References

[1] G. Bateman and D. Nelson, *Phys. Rev. Lett.* **41,** 1805 (1978)

[2] B. A. Carreras, P. H. Diamond, M. Murakami, J. L. Dunlap, J. D. Bell, H. R. Hicks, J. A. Holmes, C. E. Thomas, and R. M. Weiland, *Phys. Rev. Lett.* **50,** 503 (1983) and references therein

[3] J. R. Myra, D. A. D'Ippolito, X. Q. Xu, and R. H. Cohen, *Phys. Plasmas* **7,** 4622 (2000).

[4] J. Weiland, *Collective Modes in Inhomogeneous Plasma*, (IOP Publishing LTD Bristol; Philadelphia 2000).

[5] A. Zeiler, J. F. Drake and B. Rogers, *Phys. Plasmas* **4,** 2134 (1992).

[6] R. H. Hastie, J. J. Ramos and F. Porcelli, *Phys. Plasmas* **10,** 4405 (2003).

[7] P. N. Guzdar, J. F. Drake, D. McCarthy, A. B. Hassam and C. S. Liu, *Phys. Fluids B* **5,** 3712 (1993).

[8] B. N. Rogers and J. F. Drake, *Phys. Plasmas* **6,** 2797 (1999).

[9] X. Q. Xu, R. H. Cohen, T. D. Rognlien, and J. R. Myra, *Phys. Plasmas* **7,** 1951 (2000).

[10] A. H. Glasser, J. M. Greene and J. L. Johnson *Phys. of Fluids* **18,** 875 (1975).

[11] D. Correa-Restrepo, *Z. Naturforsch. A* **37,** 848 (1982).

[12] R. Kaiser *Nucl. Fusion* **33,** 1281 (1993).

[13] J. W. Connor, R. J. Hastie, and J. B. Taylor, *Phys. Rev. Lett.* **40,** 396 (1977)

[14] C. C. Hegna and S. R. Hudson, *Phys. Rev. Lett.* **87,** 035001 (2001)

[15] F. S. B. Anderson, A. F. Almagri, D. T. Anderson, P. G. Mathews, J. N. Talmadge, and J. L. Shohet, *Fusion Technology* **27**, 273 (1995).

[16] M. Persson, J. L. V. Lewandowski and H. Nordman, *Phys. Plasmas* **3**, 3720(1996).

[17] T. Rafiq, J. Anderson, M. Nadeem and M. Persson, *Plasmas Phys. Control. Fusion* **43**, 1363 (2001).

[18] S. P. Hirshman and O. Betancourt, *J. Comput. Phys.* **96**, 99 (1991).

[19] A. H. Boozer, *Phys. Fluids* **25**, 520 (1982).

[20] T. Rafiq and C. C. Hegna, *Phys.Plasmas* **12,** 112505 (2005).

[21] W. D. D'haeseleer, W. N. G. Hitchon, J. D. Callen, and J. L. Shohet *Flux Coordinates and Magnetic Field Structure* (Springer-Verlag, Berlin; New York, 1991) Chapt. 6.

[22] T. Rafiq and C. C. Hegna, *Phys. Plasmas* **13,** 062501 (2006).

Figure Captions:

Figure 1: (a) The ballooning mode eigenfunction as a function of θ for $\theta_k = 0$, $\hat{s} = 0.1$, $k_\theta \rho = 0.3$, $\hat{\nu_e} = 0.023$, and $\beta = 0.0002$ (left panel) and the variation of normalized growth rate as a function of ballooning parameter α (right panel). (b) Ballooning mode eigenfunctions as a function of θ for $\alpha = 0.2$ (left panel) and $\alpha = 1.0$ (right panel).

Figure 2: (a) Growth rate (left panel) and real part of the frequency (right panel) of the ballooning mode as a function of α for the RIMHD model (solid line) and the model with drift effects (DRIBM with $\triangle$ symbols) for $\hat{s} = -0.03$ and $k_\theta \rho = 0.1$. The other parameters are the same as those used in figure 1. (b) Ballooning mode eigenfunctions as a function of θ for $\alpha = 0.05$ (left panel), and 0.2 and 0.4. (right panel)

Figure 3: (a) Growth rate (left panel) and real frequency (right panel) for the DRIBM mode as a function of $\hat{s}$ for $q = 1.0$, $k_\theta \rho = 0.1$ $\alpha = 0.10$, $\tau = 1.0$, $\beta = 0.002$, $\epsilon_n = 0.07$, $\theta_k = 0$, and (b) Eigenfunctions of the DRIBM as a function of θ for positive and negative values of shear.

Figure 4: (a) Growth rate (left panel) and real frequency (right panel) for the DRIBM ($\triangle$ symbols) and RIMHD modes (solid line) as a function of $k_\theta \rho$ for $\hat{s} = -0.03$. The other parameters are the same as those used in figure 2.

Figure 5: (a) Growth rate (left panel) and real frequency (right panel) for the drift-resistive-inertia ballooning modes (DRIBM) as a function of ϵ_n for $k_\theta \rho = 0.1$, $\alpha = 2q^2\beta/\epsilon_n$. The other parameters are the same as those used in figure 2 (b) Eigenfunctions of the DRIBM are for $\epsilon_n = 0.02$ and 0.07.

Figure 6: (a) Growth rate (left panel) and real frequency (right panel) for the DRIBM as a function of β for $\epsilon_n = 0.07$, $\alpha = 2q^2\beta/\epsilon_n$, $q = 1.0$, $k_\theta \rho = 0.01$ and $\tau = 0.25$. (b) Ballooning mode eigenfunctions are plotted as a function of θ for different β values.

Figure 7: Growth rate (left panel) for the highly resistive (HR) and resistive-inertia MHD ballooning modes (RIMHD) in the electrostatic limit as a function of $(k_\perp \rho)^2$ in QHS configuration for $s = 0.8980$, $\tau = 1$, $R\nu_e/2c_s = 0.42$, $\theta_k = 0.0$, $\epsilon_n = 0.07$ and $\theta_0 = 0$, $\zeta_0 = 0$ field line. Ballooning mode eigenfunctions as a function of θ for $(k_\perp \rho)^2 = 0.24$ (right panel).

Figure 8: Growth rate (left panel) for the resistive-inertia MHD ballooning modes (RIMHD) in the electrostatic limit as a function of $(k_\perp \rho)^2$ for QHS and Mirror cases. The other parameters are the same as those used in the figure 7. (b) Ballooning mode eigenfunctions as a function of θ for $(k_\perp \rho)^2 = 0.02$ (right panel).

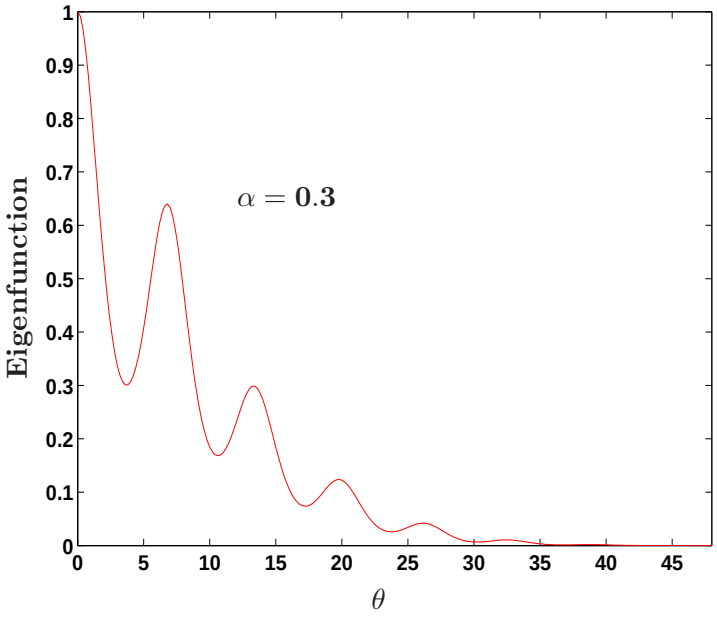

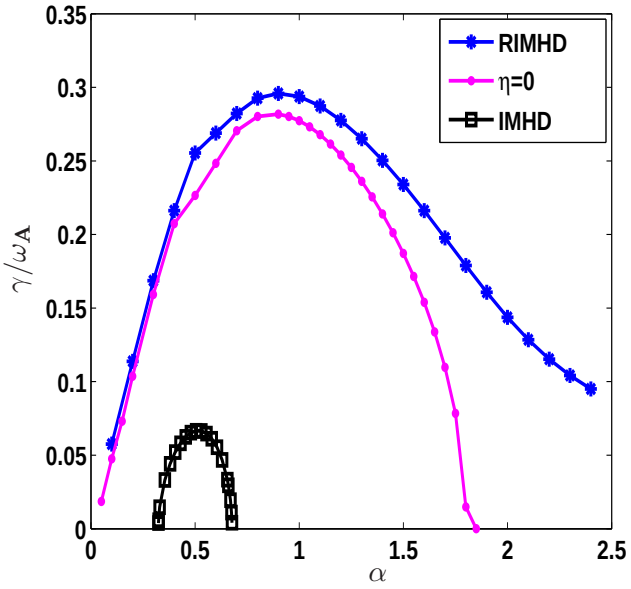

Figure1(a)

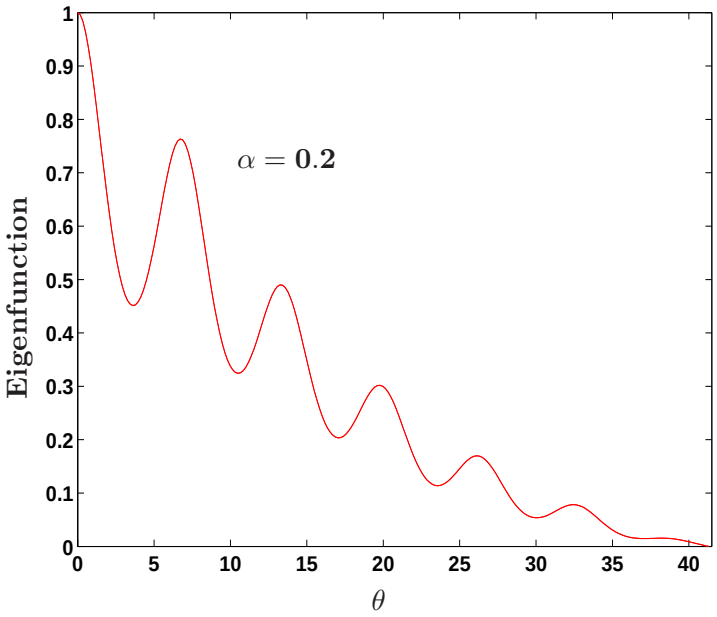

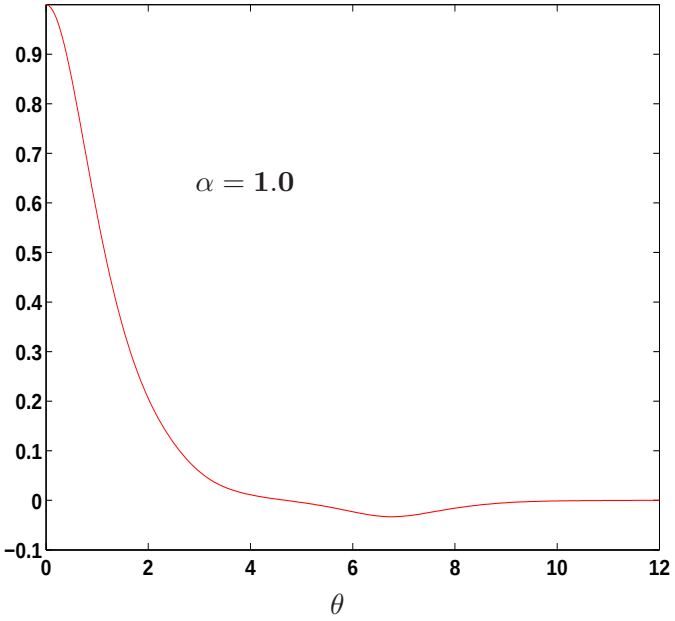

Figure1(b)

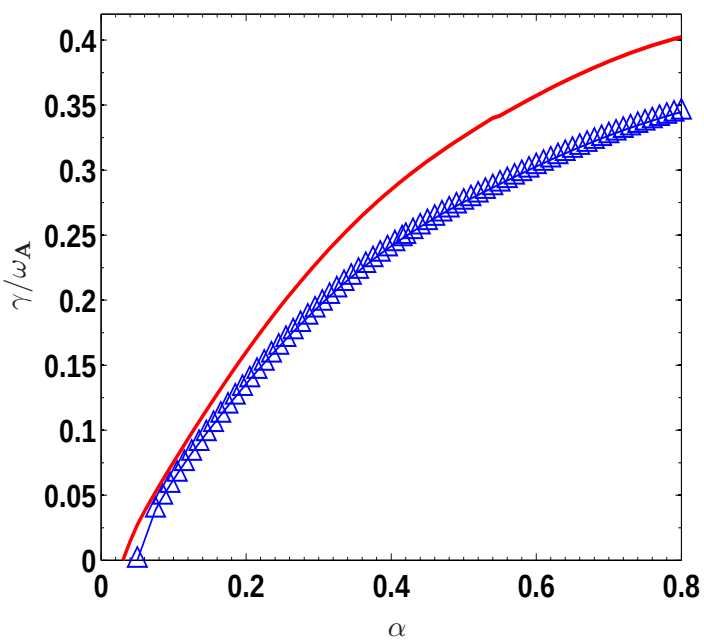

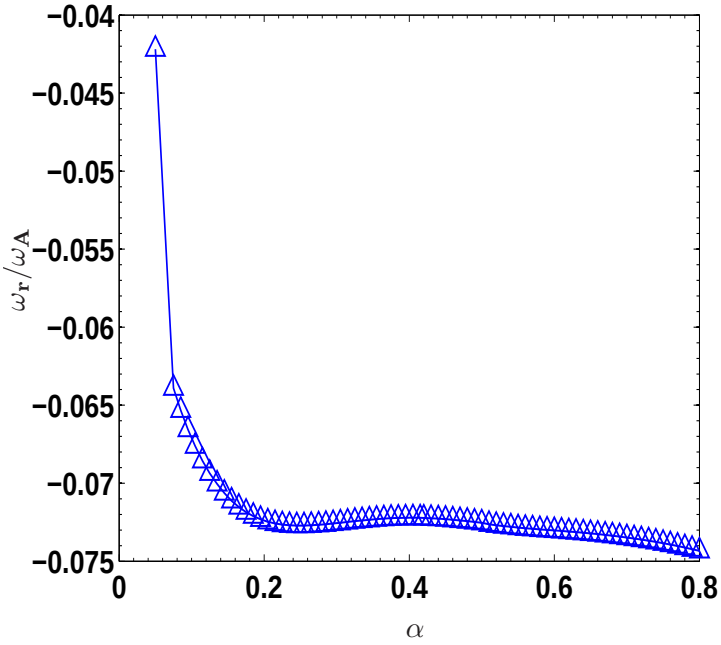

Figure2(a)

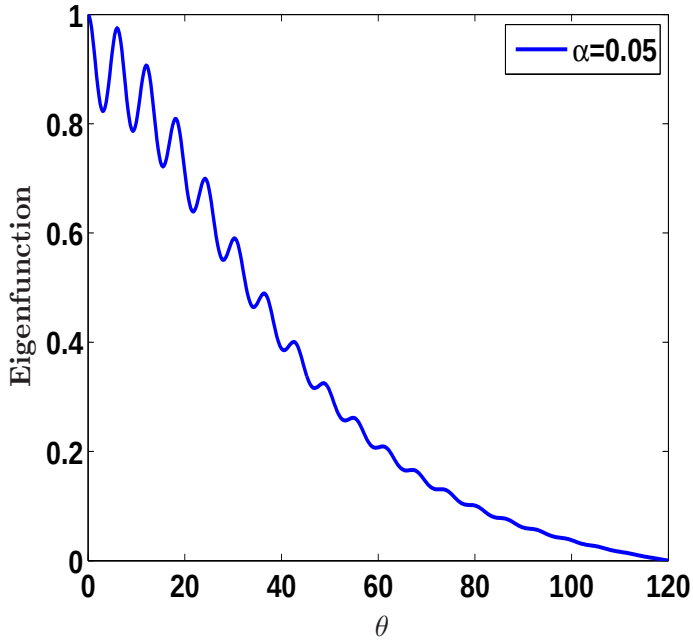

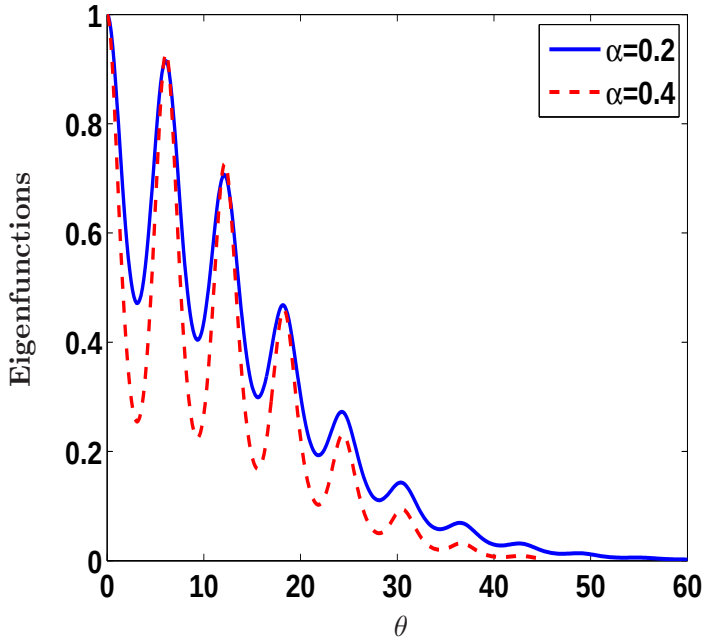

Figure2(b)

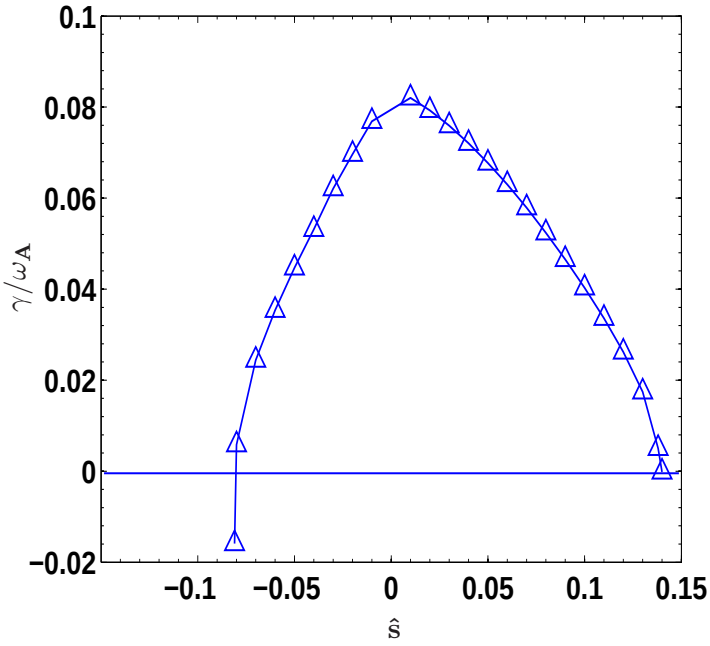

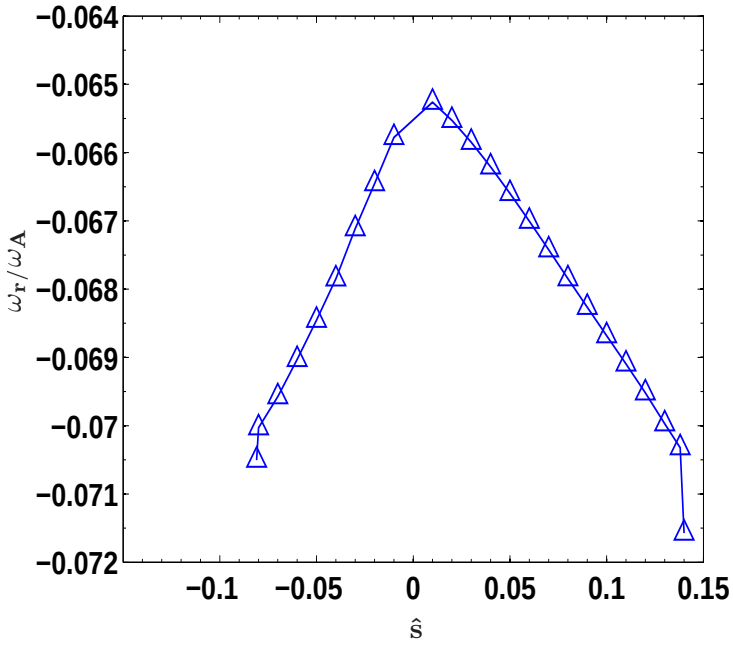

Figure3(a)

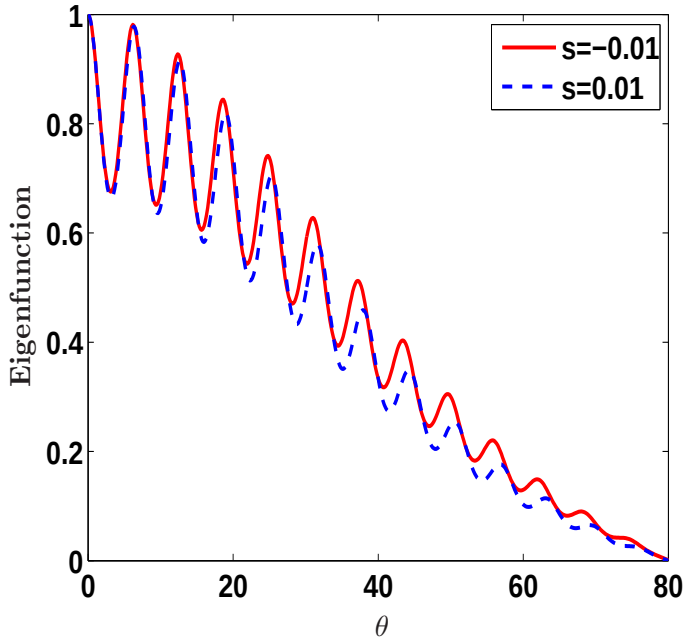

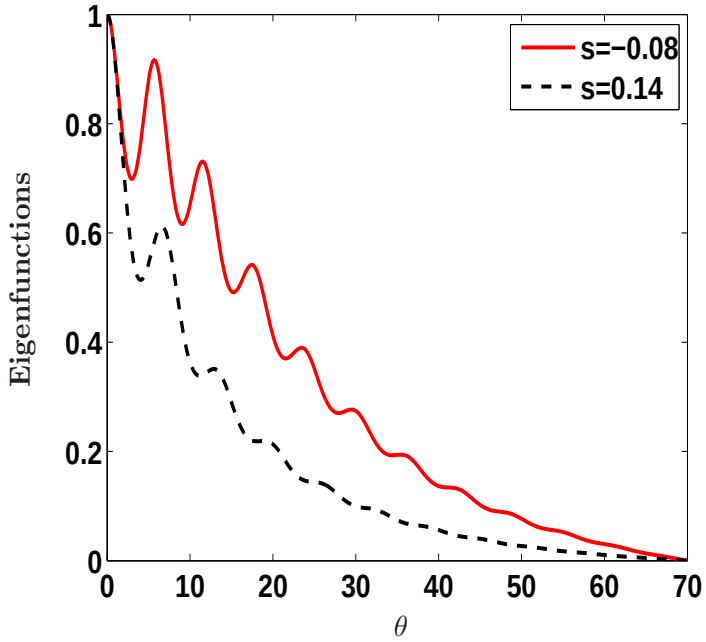

Figure3(b)

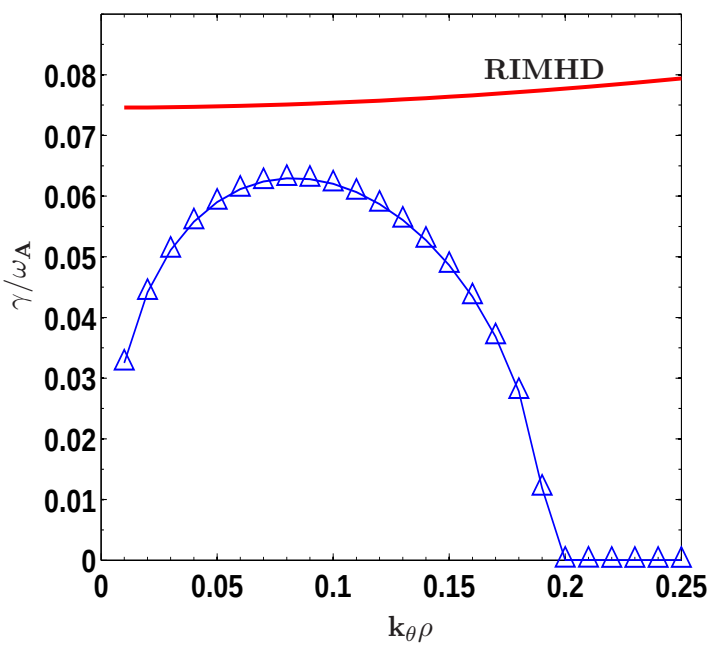
RIMHD
0.08
0.07
0.06
0.05
0.04
0.03
0.02
0.01
0
0
0.05
0.1
0.15
0.2
0.25
γ/ω_A
$k_\theta\rho$

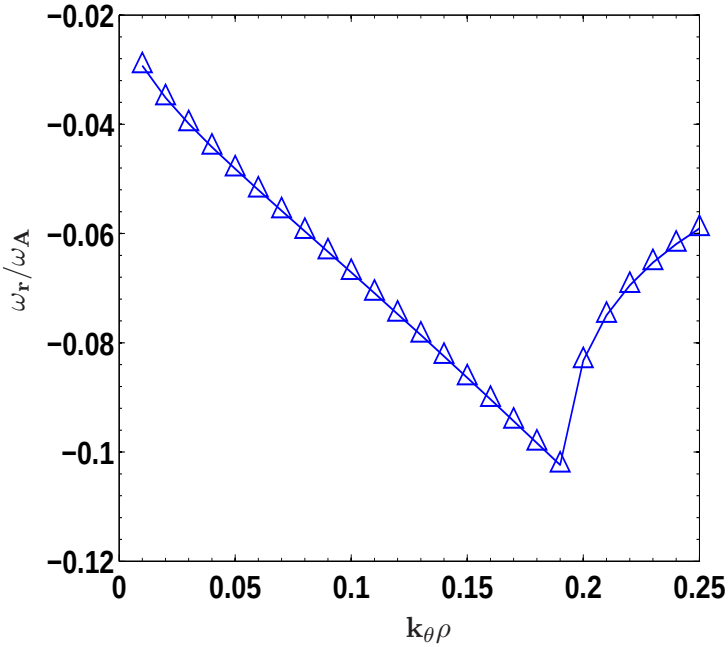
−0.02
−0.04
−0.06
−0.08
−0.1
−0.12
0
0.05
0.1
0.15
0.2
0.25
ω_r/ω_A
$k_\theta\rho$

Figure4

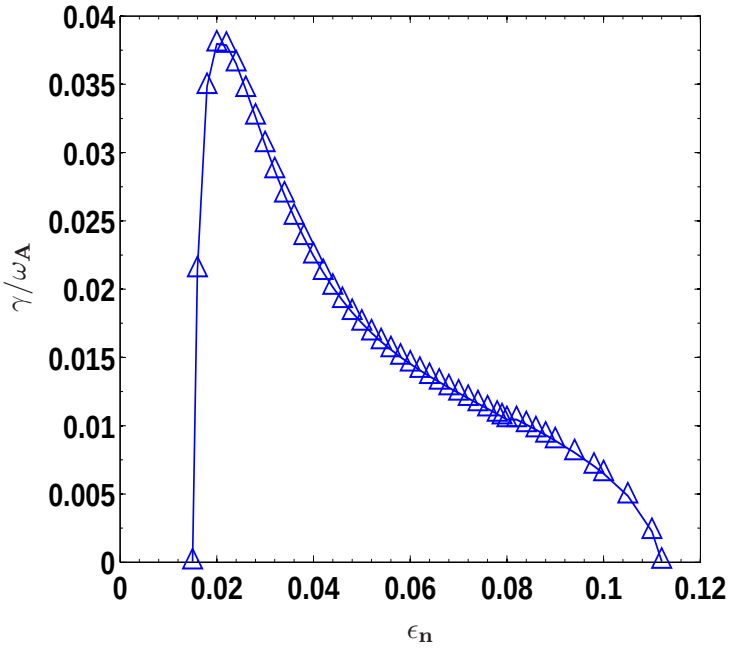

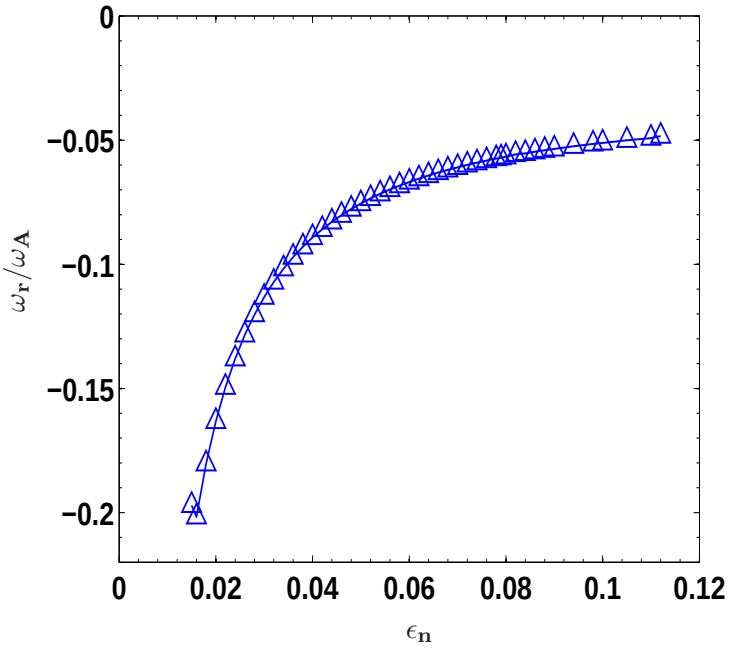

Figure5(a)

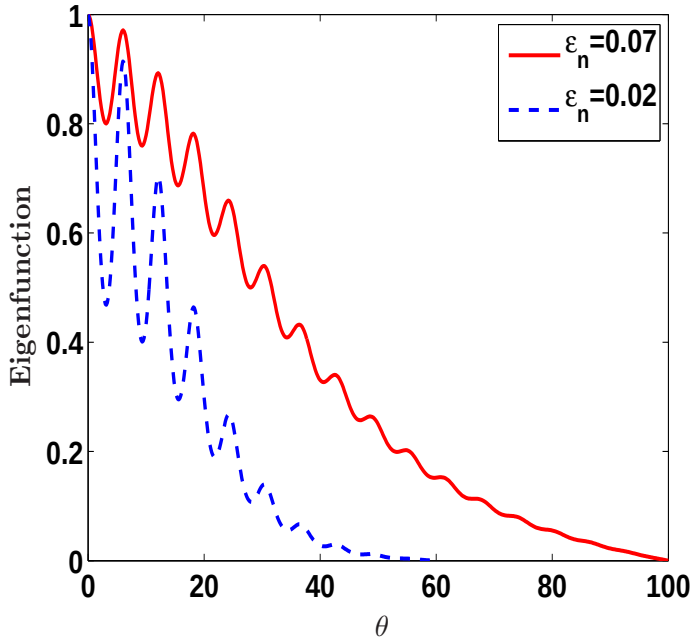

Figure5(b)

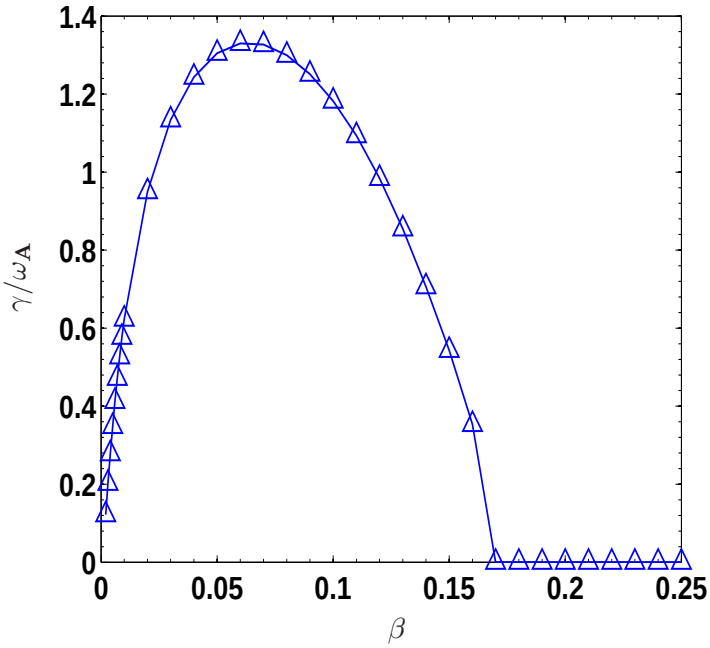

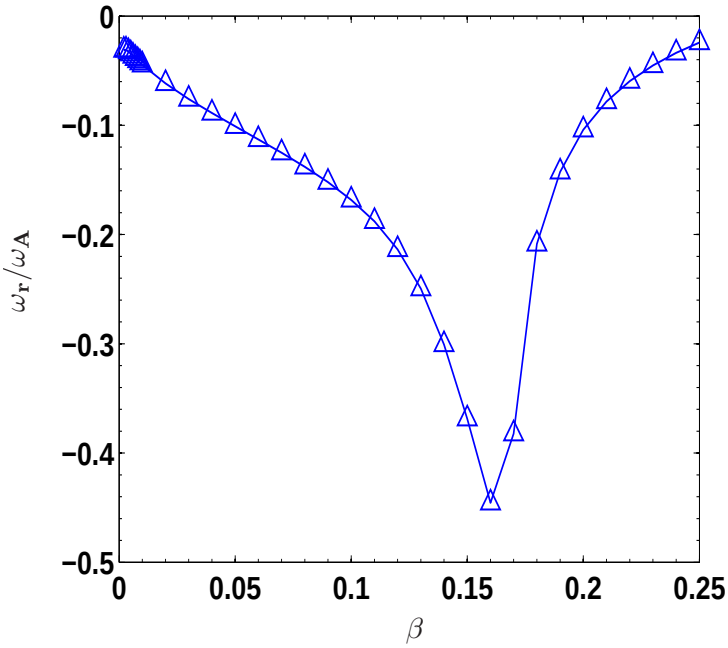

Figure6(a)

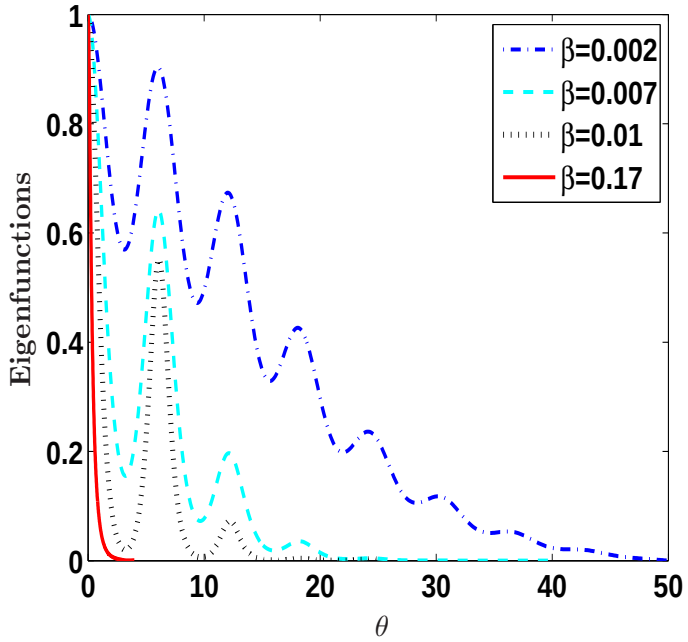

Figure6(b)

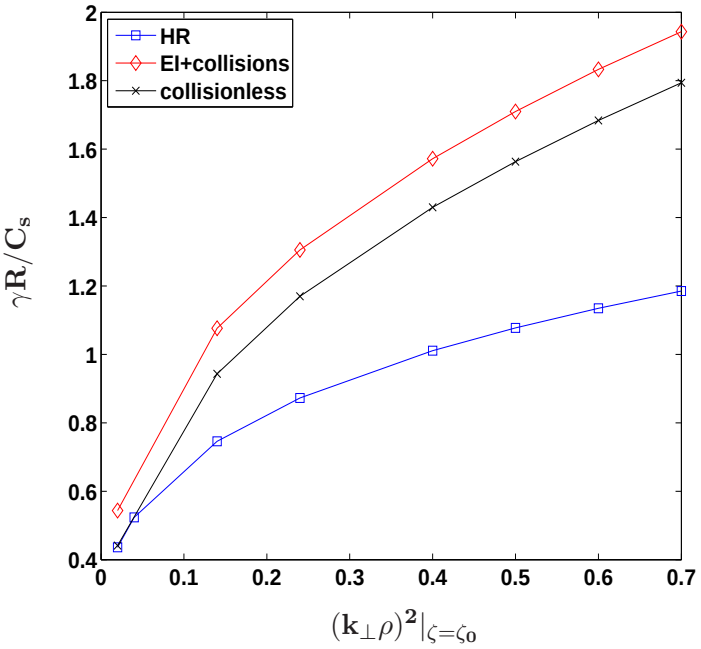
HR
EI+collisions
collisionless
$\gamma R/C_s$
$(\mathbf{k}_\perp\rho)^2|_{\zeta=\zeta_0}$

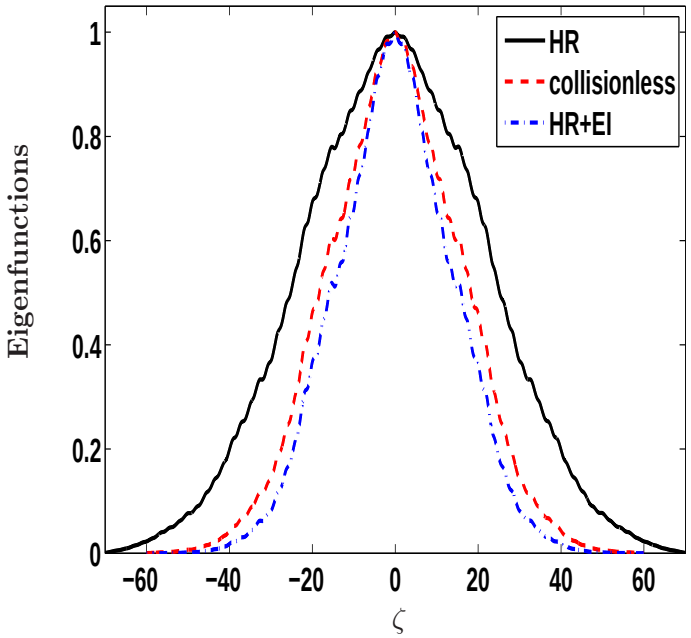
HR
collisionless
HR+EI
Eigenfunctions
ζ

Figure7

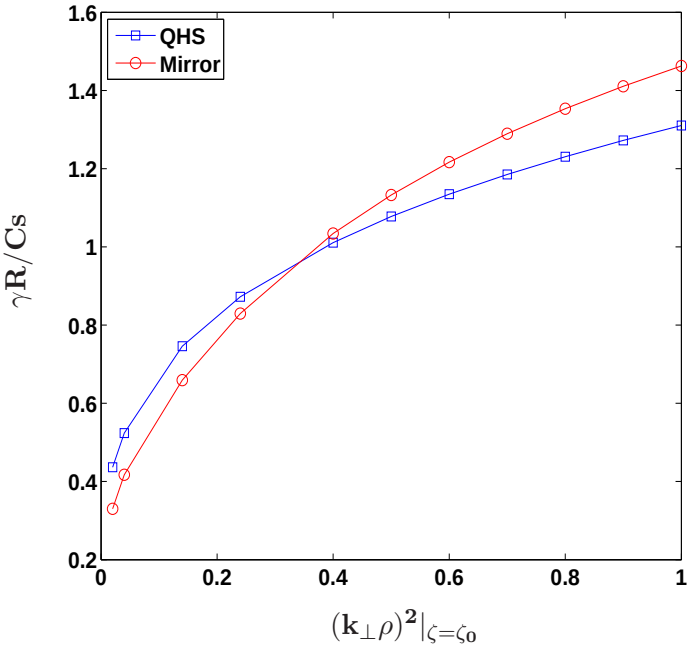
QHS
Mirror
1.6
1.4
1.2
1
0.8
0.6
0.4
0.2
0
0.2
0.4
0.6
0.8
1
$\gamma R/C_S$
$(\mathbf{k}_\perp \rho)^2|_{\zeta=\zeta_0}$

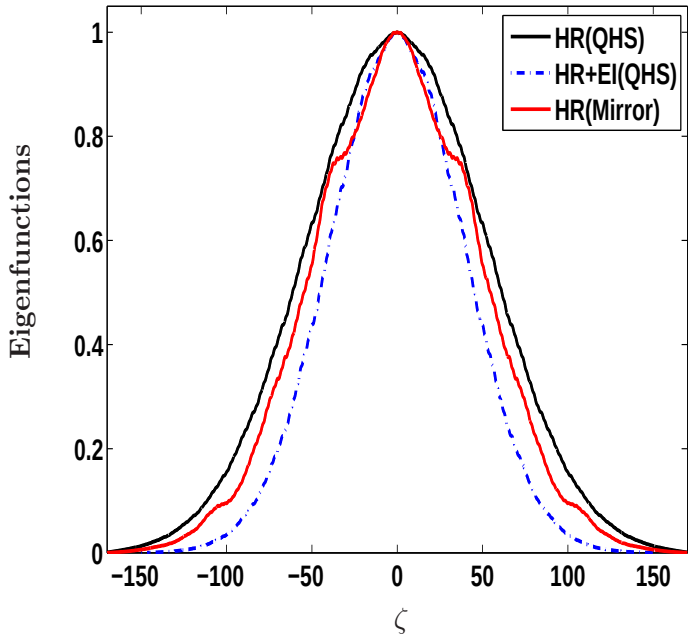
HR(QHS)
HR+EI(QHS)
HR(Mirror)
1
0.8
0.6
0.4
0.2
0
−150
−100
−50
0
50
100
150
Eigenfunctions
ζ

Figure8